Journal Pre-proof

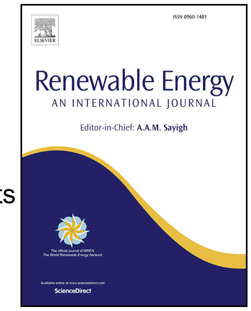

PV temperature and performance prediction in free-standing, BIPV and BAPV incorporating the effect of temperature and inclination on the heat transfer coefficients and the impact of wind, efficiency and ageing

S. Kaplanis, E. Kaplani, J.K. Kaldellis

PII: S0960-1481(21)01292-1

DOI: https://doi.org/10.1016/j.renene.2021.08.124

Reference: RENE 15935

To appear in: *Renewable Energy*

Received Date: 10 December 2020

Revised Date: 4 August 2021

Accepted Date: 30 August 2021

Please cite this article as: Kaplanis S, Kaplani E, Kaldellis JK, PV temperature and performance prediction in free-standing, BIPV and BAPV incorporating the effect of temperature and inclination on the heat transfer coefficients and the impact of wind, efficiency and ageing, *Renewable Energy* (2021), doi: https://doi.org/10.1016/j.renene.2021.08.124.

CRediT author statement

S. Kaplanis: Conceptualization, Methodology, Investigation, Resources, Writing- Original draft preparation, Writing- Reviewing and Editing. **E. Kaplani**: Methodology, Software, Validation, Formal Analysis, Investigation, Data curation, Writing- Original draft preparation, Writing- Reviewing and Editing. **J. Kaldellis**: Investigation, Validation, Resources, Writing- Reviewing and Editing.

PV temperature and performance prediction in free-standing, BIPV and BAPV incorporating the effect of temperature and inclination on the heat transfer coefficients and the impact of wind, efficiency and ageing

S. Kaplanis[1,3], E. Kaplani[2,*], J.K. Kaldellis[1]

[1] Lab of Soft Energy Applications and Environmental Protection, University of West Attica, Athens, 12201, Greece

[2] School of Engineering, Faculty of Science, University of East Anglia, Norwich, NR4 7TJ, UK

[3] Renewable Energy Systems Lab, University of Peloponnese, 26334 Patra, Greece

email addresses: skaplanis@uniwa.gr, e.kaplani@uea.ac.uk, jkald@uniwa.gr

*Corresponding Author

Abstract

A novel compact model is developed to predict the PV temperature T_{pv}, coefficient f which relates T_{pv} with the in-plane solar irradiance I_T, and power output P_m. The T_{pv}, I_T, ambient temperature T_a, and wind velocity v_w on a sun-tracking pc-Si PV and c-Si BIPV were monitored. f depends explicitly on v_w, PV efficiency, heat losses coefficient, and implicitly on T_{pv}, I_T, T_a, loosely on the module inclination at low v_w, while this effect weakens at high v_w. T_{pv} prediction is provided by means of 5 functions, which cater for the deviation of the environmental conditions from the Standard Operating Conditions, the operating efficiency, the natural ageing, PV geometry and cell technology. The T_{pv} prediction for the sun-tracking system has relative error 2.6% for PV operating temperatures around the NOCT, and may overestimate by up to 1.4°C. Similarly, the relative error for the BIPV system is -2.1% for PV temperatures around the NOCT, with underestimation up to 1.6 °C. The model predicted P_m with relative error 1.9% for PV operating near its nominal value. The model is compared to 3 well-known models and also applied to other BIPV/BAPV configurations in various countries proving its wide applicability, high accuracy and universality.

Keywords: PV temperature prediction, PV power prediction, BIPV, temperature and wind effect, inclination effect, PV ageing

Nomenclature			
BAPV	Building Adapted PV	T_{sky}	sky temperature (K)
BIPV	Building Integrated PV	U_f	heat losses coef. due to convection and IR radiation at the front side of the PV module (W/m^{2}K), equal to $h_{c,f}+h_{r,f}$

$F_{pv\text{-}sky,f}$ $F_{pv\text{-}gr,f}$	View factor of the front PV surface to sky and to ground, respectively	U_b	heat losses coef. due to convection and IR radiation at the back side of the PV module (W/m^2K), equal to $h_{c,b}+h_{r,b}$
$F_{pv\text{-}sky,b}$ $F_{pv\text{-}gr,b}$	View factor of the back PV surface to sky and to ground, respectively	U_{pv}	The overall heat losses coefficient from a PV (W/m^2K), equal to U_f+U_b
Gr	Grashof number	$U_{pv,SOC}$	U_{pv} at SOC (W/m^2K)
I_T	Global solar radiation intensity on the PV plane (W/m^2)	f	Coefficient relating PV module temperature with ambient temperature and solar irradiance on the PV plane
$I_{T,SOC}$	Global solar radiation intensity at SOC conditions, 800 W/m^2	$h_{c,f}$	heat convection coefficient from PV glass to air (W/m^2K)
$I_{T,ref}$	Reference solar irradiance equal to 10^3 W/m^2	$h_{r,f}$	Radiative heat coefficient from the front PV side (W/m^2K)
L	length of the PV module in the direction of the air flow along its front or back side, or as otherwise stated in the text (m)	$h_{c,b}$	heat convection coefficient from PV back surface to air (W/m^2K)
NOCT	Nominal Operating Cell Temperature	$h_{r,b}$	Radiative heat coefficient from the PV back side to environment (W/m^2K)
Nu	Nusselt number of the air flow either in the front or back side of the PV module, to be stated	k_i	thermal conductivity of material i (W/mK)
P_m	maximum power output at operating conditions (W)	r_{ageing}	percentage of overall degradation due to ageing
$P_{m,STC}$	maximum rated power at STC (W)	v_w	wind velocity (m/s)
$P'_{m,STC}$	maximum power at STC for the year of operation (W)	ΔT	Temperature difference between PV and air bulk temperature, T_{pv}-T_o
$P_{m,sys}$	final power output of the PV system	$\Delta T_{c\text{-}b}$	Temperature difference between cell and back, T_c-T_b
Pr	Prandtl number	β	PV module inclination angle with reference to horizontal
$\dot{Q}$	the normalized to m^2 heat rate (W/m^2)	δT_{pv}	Difference between the PV temperature and its temperature at SOC, T_{pv}-T_{SOC}
Ra	Rayleigh number, Ra = Gr Pr	δx	Layer thickness (m)
SF	Scaling factor multiplied with f to adapt the model to BIPV/BAPV configurations	ε_{losses}	percentage of power conditioning losses at system level
SOC	Standard Operating Conditions	ε_{sky},ε_{pv}, ε_b, ε_{gr}	emissivity coefficients for the sky, the PV glass, the back surface and ground respectively
STC	Standard Test Conditions	η_{pv}	PV module nominal efficiency
T_{pv}, T_c T_f, T_b	PV module temperature, PV semiconductor temperature, PV front side and PV back side temperatures, respectively	$\eta_{pv,SOC}$	module efficiency at SOC in the year of operation for the module used in the development of the model
T_{pl}	the indoor plank/plaster temperature	$\eta_{pv,STC}$	module efficiency at STC in the year of operation
T_a	ambient temperature (ºC or K as specified)	$\eta_{pv,n}$	efficiency at SOC for the module to be tested
T_{bl}	film temperature of the air boundary layer at the PV module side front or back (K)	θ	PV module inclination with respect to vertical
T_{gr}	ground surface temperature (K)	ν	kinematic viscosity of the air (m^2/s)

1. Introduction

The development of temperature profiles, T_{pv}, in PV modules operating in field conditions was studied since many years due to its importance on the PV performance studies. Various formulas have been proposed as outlined in [1] as it concerns the T_{pv} and the power output, P_m, prediction. The T_{pv} profiles are well understood by building a simulation model based on the Energy Balance Equation (EBE), for transient and/or steady state conditions, taking into account the power and heat generated within a PV module operating under a global solar radiation intensity on it, I_T, at ambient temperature, T_a, and wind speed, v_w [2-9]. A large number of research articles deal with the prediction of the PV module or PV cell temperature T_{pv} and T_c, respectively, for cell types such as mc-Si, pc-Si, a-Si, CIS, CdTe [10] providing comparisons with other models and with measured values and investigating the effect of various external factors, as discussed below. In [11-14], the differences between T_{pv}, T_c, T_b and T_f which stand for the module temperature, the cell semiconductor layer temperature, and the module's back and front side temperatures, are argued. T_b is measured in the experiments and is usually referred as T_{pv} or T_m. Finally, T_c is estimated [11]:

$$T_c = T_b + \frac{I_T}{I_{ref}} \cdot \Delta T_{c-b} \qquad where\ \ \Delta T_{c-b} = T_c - T_b \tag{1}$$

I_T is the intensity of the global solar radiation on the module and $I_{ref}=10^3$ W/m^2. The value of $\Delta T_{c\text{-}b}$ is taken equal to 2-3ºC according to [11,12], while in [6] the ΔT difference was defined instead as (T_f -T_b) equal to 3ºC. Based on the heat flow continuity from the semi-conductor to the PV back side the following formulas may be used to determine T_c from T_b which is the temperature usually measured.

$$T_c = T_b + \dot{Q} \cdot \Sigma(\delta x_i/k_i) = T_b\left(1 + \frac{\Sigma(\delta x_i/k_i)}{U_b{}^{-1}}\right) - T_\alpha \frac{\Sigma(\delta x_i/k_i)}{U_b{}^{-1}} \tag{2}$$

$\dot{Q}$(W/m^2) may be assumed to a good first approximation as half of the heat rate generated in the semiconductor, in glass-glass or glass-tedlar module technology, estimated equal to $0.5(1-\eta_{pv})/I_T$ neglecting a small fraction of reflected radiation. This assumption is valid because the heat conduction resistance from the cell to the front and to the back side and the corresponding convection and radiative heat coefficients do not differ so much to each other. $\Sigma(\delta x_i/k_i)$ is the total resistance per m^2 due to heat conduction in the layers from the semiconductor to the back surface and U_b is the heat losses coefficient (convection and radiated heat) from the PV back surface. For insulated PV back surfaces or low U_b both expressions in eq.(2) result to $T_c=T_b$. Giving appropriate values to the physical quantities [5,6], in eq.(2) results to $\Delta T_{c\text{-}b}=T_c - T_b=2$ºC for $I_T=10^3$W/m^2. This value depends also on the material of the cell layers, i.e. their conductivity coefficients and their thickness and also on the wind speed which strongly affects U_b. The assumption $T_c=T_b=T_f$ in [15] is a gross approximation which has to be argued on the basis of the difference between predicted and measured T_b which for most models is higher than the expected intra-cell temperature difference, $\Delta T_{c\text{-}b}$=2-3ºC.

In the group of physics-based models for the T_c prediction a set of equations is formulated including the EBE at steady and/or transient conditions coupled with equations on heat propagation from the semiconductor layer to the front and back surfaces and then to the environment [3,7,16,17]. It is important to take into account the radiated heat exchanged between PV surface and sky/ground. Such a set of equations which take into account all the environmental conditions constitute a complete simulation model [2,3,8,9,18-20]. However, the heat convection and the radiated heat coefficients used do not cover sufficiently the whole range of the environmental conditions. More elaborated analysis was outlined in [3,17,21,22] and provided better T_c predictions. In a second group, the so called grey models, electric and heat transfer parameters associated to the operating PV module are introduced into an EBE and a regression analysis of recorded data from monitored quantities is applied for the development of semi-empirical models for T_c prediction. Those (semi)-empirical T_{pv} prediction models are categorized as explicit and implicit ones. Implicit models are the ones which provide T_{pv} through variables which depend on the T_{pv} itself as it is the PV efficiency, η_{pv} and the heat losses coefficients, U_f, U_b or $U_{pv}= U_f + U_b$. The latter coefficients are T_{pv} dependent mainly due to the radiative heat coefficients, $h_{r,f}$ and $h_{r,b}$ for the front and back PV side and strongly dependent on v_w through the heat convection coefficients, $h_{c,f}$ and $h_{c,b}$, for the front and back PV module sides, respectively. $h_{c,f}$ and $h_{c,b}$, are loosely dependent on T_{pv} and T_a. The most common T_c or T_{pv} prediction empirical formulas of explicit and implicit structure which appear in PV performance model comparisons [1,12,19-24] take the forms summarized in Table 1.

Table 1: PV temperature prediction explicit and implicit empirical models

Model	Reference	Equation
$T_c = T_a + \frac{I_T}{I_{T,NOCT}}\left(T_{NOCT} - T_{a,NOCT}\right)F\left(U_{pv}\right)F'\left(\frac{\eta_{pv}}{T_a}\right)$	[13,14,25,26]	(3)
$T_c = T_a + \frac{I_T}{I_{T,NOCT}}\left(T_{NOCT} - T_{a,NOCT}\right)\frac{U_{pv,NOCT}}{U_{pv}}\cdot\left(1 - \frac{\eta_{pv}}{(\tau\alpha)}\right)$	[1,13]	(4)
$T_c = T_a + fI_T$	[27-29]	(5)
$T_c = T_a + aI_T(1 + \beta T_\alpha)F(v_w)F'(\eta_{pv})$	[30]	(6)
$T_c = T_a + \frac{I_T}{(U_o + U_1 v_w)}$	[31,32]	(7)
$T_c = T_a + I_T \exp(a + bv_w)$	[11, 33]	(8)

In the above models, the thermal radiation exchanges between the PV module and the environment were not adequately considered despite the considerable temperature difference between the PV module and the sky-ground environment. The assumption argued in [13], by which a T_c prediction model, eq.(3), might be converted from implicit to explicit, by dropping the factors $F(U_{pv})$ and $F'(\eta_{pv}/(\tau\alpha))$ as not essentially affected by T_c and v_w, is not always valid because v_w and T_c may take values which substantially affect the T_c result. Deviations between the predicted T_c values by various models and measured ones are shown in [23,24,34]. It was concluded that the NOCT model outlined in [35] deviates more as it does not take into account the v_w effect, while the rest of the aforementioned models consider a linear dependence of $h_{c,f}$ and $h_{c,b}$ on v_w. However, these do not fit well in the whole range of v_w values as discussed in [17], where the PV module geometry and the wind speed and direction have to be taken into account in order to predict the parameter f introduced in eq.(5), which is known as the Ross coefficient and relates T_c with T_a and I_T [27] .

A third group of methodologies applies ANN for the T_c prediction resulting in eq.(9), [22,36,37]. T_c is predicted as a function of T_a, I_T, v_w, wind direction and humidity. In the ANN approach it is necessary to train the model to the site environmental conditions, the specific mounting scheme, the structural details, geometry and the type of PV cell, in order to obtain suitable parameters for the T_c prediction, independent, if possible, of the site and the technology type, as claimed in [36].

$$T_{pv} = 0.943T_a + 0.028I_T - 1.528v_w + 4.3 \tag{9}$$

In [24], a T_c prediction formula different to eq.(9) has been derived through ANN for the floating PV modules. This justifies the argument on the specific training requirements for the ANN methodologies applied for the T_c prediction and that a general purpose T_c prediction model is absolutely required.

An investigation of the v_w effect on T_{pv} ,(practically equal to T_b and T_c), η_{pv} and P_m was outlined in [34,38-41] where the models [13,14,32,33] and the NOCT were applied in mc-Si, pc-Si, a-Si and CdTe modules. The factors U_o and U_1 used in [32] were adopted from [31]. The NOCT model provided higher values as it does not take into account the v_w effect in the module cooling, as mentioned above. The other models exhibited coefficient of determination, R^2, between predicted and measured T_c from 0.85 to 0.96. However, the implicit nature expressed by $T_{pv}(I_T,T_a,\eta_{pv}(T_{pv},I_T,v_w),U_{pv}(T_{pv},I_T,v_w))$, the module inclination, and the wind direction have not been considered adequately enough. Indeed, v_w, and I_T, have a 2nd order effect on T_{pv} through their effect mainly on η_{pv} and U_{pv} and this has to be accounted for. In [42], the role of I_T, v_w, T_a and the solar spectrum in the PV performance, as well as their impact on T_{pv} in c-Si and CdTe cells have been studied taking into account the coefficients U_o and U_1 [31,32]. A simpler T_{pv} implicit formula was developed [14] based on the EBE taking into consideration T_{pv} dependent PV coefficients and not the NOCT as it was done in [11,25]. In the above referenced models, the PV heat losses coefficient $U_{pv}(v_w)$ was assumed to be linearly dependent on v_w which does not hold for natural heat air flow as it was analytically presented in [17,21].

Additionally, Building Integrated PV (BIPV) in roofs or facades attracted a lot of research interest, since they behave as distributed clean energy sources towards zero energy buildings, presented in review papers [43-45]. Similarly, Building Adapted PV (BAPV) design configurations have been studied for roofs and sunshades [46-48]. Fig. 1 shows BIPV and BAPV designs on roofs and facades, the former representing fully integrated PV solutions into the building structure and the latter building adapted solutions with a naturally ventilated air gap between the PV modules and the building elements. The T_{pv} prediction is one of the main objectives in the design of BIPV and BAPV because it affects significantly the PV performance. Also, BIPV/T configurations have been investigated [49-51]. Several simulation models have been developed for the various BIPV, BAPV, BIPV/T configurations per case, and comparisons of predicted T_{pv} values with experimental data gave very good results [50-52]. However, an extended validation process applying those simulation models to any other environment and BIPV design has been limited mainly due to the complexity of the simulation models and their use of parameters specific to the particular BIPV design studied. In most of the BIPV, BAPV, BIPV/T works published [15,46, 53-54] the experimental results and the models developed have been compared to widely accepted and applicable simple formulas and software such as [11,13,53,55]. While the benefit of a general formula for T_{pv} prediction is obvious, there is a great necessity for increasing the accuracy of T_{pv} prediction taking into account important parameters, which are missing from simple widely accepted models.

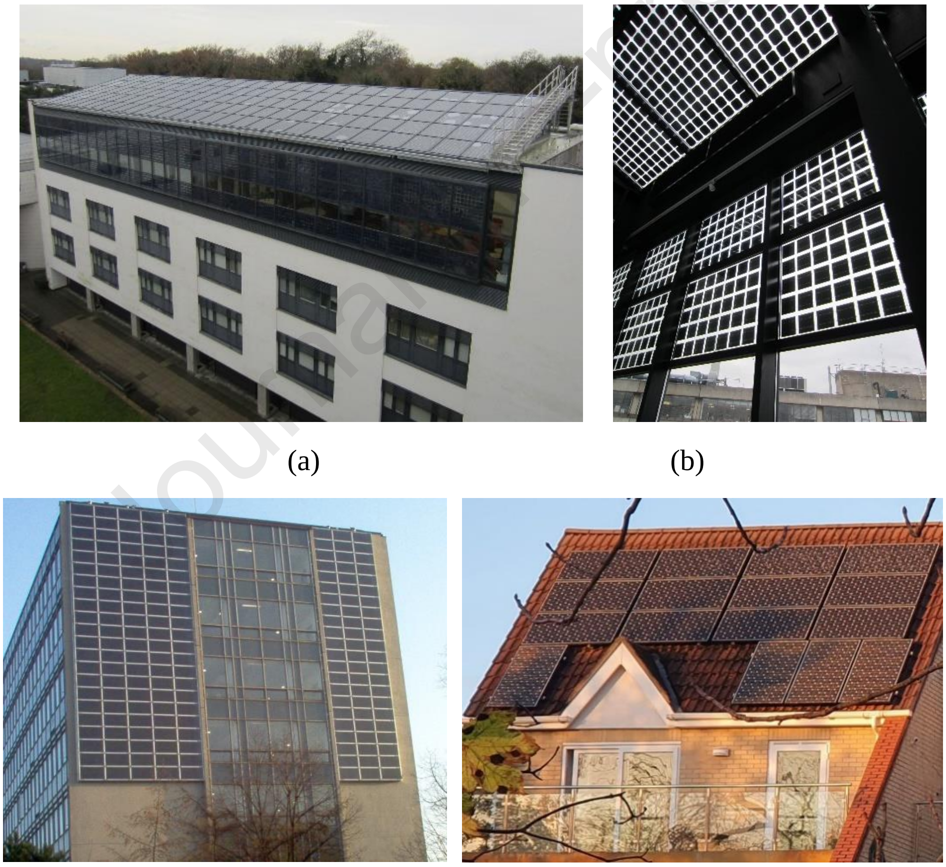

(a) (b)

(c) (d)

Fig. 1. (a) BIPV at the South facing façade and rooftop of ZICER building at the University of East Anglia, UK, (b) an interior view of the BIPV façade and rooftop of ZICER building shown in (a). The BIPV façade and rooftop consist of glass/glass pc-Si and sc-Si PV modules respectively, (c) BAPV on the SW facing façade with 10cm wide air gap between the c-Si PV modules and the building wall at the Czech Technical University in Prague, (d) BAPV mounted on the rooftop with a small air gap between the PV modules and the roof tiles at a residential building in Norwich, UK.

This research study aims to fill in this gap and develop a rigorous, innovative, flexible and compact model and integrate the effect of the v_w on T_{pv} and U_{pv}, the effect of T_{pv} on η_{pv} and U_{pv}. Also, the effect of I_T on η_{pv} and the effect of the PV inclination β on the U_{pv}. The latter is essential especially in the study of BIPV facades. All these important effects have not been previously considered in a generalized compact model for T_{pv} and P_m prediction. An additional parameter of importance is the PV mounting design, either for free standing, or BIPV, BIPV/T and BAPV as it significantly affects T_{pv} and the air flow past one or both PV sides. The model developed in this study integrates all the above and takes into account the module efficiency and its natural ageing which are responsible for deviations observed between predicted and measured T_{pv}.

In Section 2, the PV configurations used in this study for the model development and validation are described along with the experimental details, while in Section 3, heat transfer issues of the PV configurations are discussed along with a short analysis to derive the formulas for the coefficients of heat convection and radiated heat from the PV modules to the environment and the estimation of their rates of change with respect to temperature T and inclination β. In Section 4, a detailed analysis for the development of the T_{pv} prediction model is presented. The mathematical expressions which take into account the above mentioned conditions are provided. In Section 5, results of the proposed model for free-standing and BIPV are presented and discussed while the model itself is validated by comparing the predicted T_{pv} and P_m values with experimental ones and with results from other models [11,31,36].

2. PV configurations and experimental procedure

Two main PV configurations were used in this study, a free-standing and a building integrated PV operating in the RES Lab, University of Peloponnese in Patra, Greece. The first one is a double axis sun-tracking PV system 480W_p shown in Fig.2(a-b) together with an identical fixed –angle PV array South facing and inclined at $\beta \approx \varphi = 38^o$ which was additionally used for model development. The fixed and sun-tracking PV systems consist of 4 pc-Si Energy Solutions modules, each 120W_p with dimensions 1.490m x 0.674m, and 9 years of operation. The parameters monitored for a period of 2 years include the T_{pv} measured at the back side of the modules with Cu-Const thermocouples, the solar irradiance on the PV plane I_T measured with Kipp & Zonen CM11 pyranometers mounted on the plane of the PV modules, the ambient temperature T_a measured via means of a MP101A sensor, the wind velocity v_w and wind direction monitored using a R.M. Young 05103 anemometer 4m above the PV system. The wind speed was converted to the level of the modules by using the Justus and Michail formula [56]. The sun-tracking PV system was monitored via an in-house developed system including an electronic load and capturing the I-V characteristic of the PV generator during 4 cycles at the beginning of every hour. The peak power P_m was then extracted from the I-V characteristic. The PV related parameters were monitored for a period of 4 min at the beginning of every hour with sampling rate 500ms and were combined with the corresponding recordings of the environmental parameters monitored in 1 min intervals with the synchronized meteo-station in the laboratory. The recordings were logged via means of 2 synchronized Campbell Scientific CR1000 data loggers, and 4 min averages were calculated. The data were previously screened for clear sky days for a more reliable representation of the *f* coefficient as the generalized model developed is steady-state. The range of conditions recorded are: T_a from 3.8 to 37°C, I_T from 94 to 1104 W/m^2, v_w from 0 to 8.5m/s. The wide range of inclination and orientation angle achieved by the sun-tracking system throughout the days and year allowed the robust validation of the model.

For the sun-tracking PV system with 9 years of operation in the field, data from the 8th year of operation were used for the model development for which a 9% degradation and a 0.11 efficiency at STC were considered, while data from the 9th year of operation were used for the model validation considering a 10% PV degradation experimentally determined.

The BIPV configuration is 110W$_p$ consisting of 2 c-Si SIEMENS SM55 modules integrated in the roof of an experimental test cell shown in Fig.2(c-e) alongside with a building integrated solar collector on the roof and the façade of the test cell. The BIPV test cell with dimensions (W, L, H) 2.8m x 2.8m x 1.75-2.5m has inclination 15° and orientation 10°SW. The dimensions of each module are: 1.293m x 0.329m. The parameters monitored in the BIPV include T_{pv} measured at the back of the modules using Cu-Const thermocouples, the irradiance at horizontal and the diffuse irradiance measured with Kipp & Zonen CM11 pyranometers and were used to convert to the irradiance on the inclined PV plane. Meteorological parameters T_a and v_w, were measured with the meteo-station and the v_w converted to 3m height with the aforementioned formula. The two data-loggers of the systems were synchronised and data were recorded in 1 min intervals. The BIPV data captured for the duration of 32 days across the months April, May, June include varying conditions during clear sky, partly clouded and cloudy days. The range of the conditions recorded in the 1 min intervals are: T_a from 6.6 to 37°C, I_T from 0 to 1132 W/m^2, v_w from 0 to 8.2m/s. The BIPV unit has 14 years of operation in the field and 13% degradation is experimentally determined. Their STC efficiency at present status is η_{pv}= 0.113 compared to their nominal value 0.129.

(a) (b)

(c) (d) (e)

Fig.2. (a) fixed-angle and sun-tracking PV array, (b) back side of sun-tracking PV array, (c) BIPV with the PV modules integrated in the roof, (d) the back side of the PV modules in the BIPV test cell with wooden case removed to reveal the back of the modules (e) the end of the wooden case forms an air orifice profile for the heated air to be exhausted through the solar chimney or self-circulated in the room.

The design of this BIPV test cell is based on a concept similar to a naturally ventilated BIPV/T [57]. T_{pv} profiles have been studied in similar designs [47-55,58-61], with the modules directly mounted on the roof tiles or at a small distance above them, off-roof. Heat from the PV front side may be extracted by free, mixed or forced air convection in contrast to the wind protected BIPV back side as outlined in [43,45,62-63]. Wooden planks are placed 18cm below the PV backside (these have been removed in Fig.2(d) to show the back of the PV modules) and form the ceiling of the BIPV, which operates as a PV/T with the heat extracted by natural convection of the warm air self-pumped due to temperature difference with the indoor temperature through an orifice pattern (Fig.2(e)). In warm days, the air is self-pumped out of the BIPV through a solar chimney. Similar designs have been studied with regard to T_{pv} profiles and thermal performance of building in [64-67]. Both sides of the modules experience radiated heat exchange with sky, ground and indoor walls estimated using the view factors, $F_{i\text{-}j}$ and the $h_{r,f}$ and $h_{r,b}$ coefficients.

The estimation of the h_c and h_r done in [17,65,68-73] is not required in this model. Their effect is integrated into a *f* function which incorporates deviations of actual field conditions from the average environmental conditions: I_T=800 W/m^2, T_a=20^{o}C, v_w<1m/s (SOC) and for β=φ=38^o. Corrections to the *f* or T_{pv} prediction are introduced using the rates of change of the above coefficients with respect to the deviations of I_T, T_{pv}, η_{pv}, T_a, v_w from their SOC values and of β from β_{ref}=38°.The rates of change of $h_{c,f}$, $h_{c,b}$, $h_{r,f}$, $h_{r,b}$ vs T_{pv} and β, are discussed in Section 3 and integrated in the model in Section 4. These rates of change contribute essentially to the accurate prediction of the T_{pv} profiles.

3. The heat convection and radiated heat coefficients and their rate of change with respect to PV temperature and inclination

3.1 The natural heat convection coefficients $h_{c,f}$ and $h_{c,b}$ for the front and back PV sides

Nu expressions valid for the entire range of the Ra number, Ra=Gr·Pr are critically discussed in [17] for the estimation of $h_{c,f}$ and $h_{c,b}$ for any heat transfer mode The transition to turbulent is determined by the critical Grashof number, Gr_c. This phenomenon depends on β or θ which is the angle between the vertical and the module. β+θ=90°.

The transition for facing down heated planes occurs at $Gr_c=3x10^{11}$ for θ=75°, $2\cdot10^{10}$ for 60°, 10^9 for 45°, $7\cdot10^7$ for 30° and $4\cdot10^6$ for 15° [74]. The Gr_c for the facing upward heated plate is lower: $5\cdot10^9$ for θ=15°, $2\cdot10^9$ for 30°, 10^8 for 60° and 10^6 for 75° [70].

3.2 The transition from laminar free convection to turbulent in the PV front and back sides

The transition to turbulent at various β needs to be examined especially for BIPV and BAPV. Let T_{pv} =60°, T_a=20°C, and the SM55 module length, L=1.33m. Also, $Gr = g\cdot\cos(\theta)\cdot\beta'\cdot(\Delta T)\cdot x^3/\nu^2$. For θ=75° or β=15°, and boundary layer temperature, T_{bl}= (60°+20°C)/2=40°C, β'=1/(273+40) and for ΔT =T_{pv}-T_a=60°-20°C, the value of $g\cdot\cos(\theta)\cdot\beta'\cdot\Delta T/\nu^2$ is calculated equal to $11{,}150\cdot10^4$. The Gr_c criterion for the back side gives transition to turbulent at x=6.3m > L. Hence, the air flow in the BIPV back side is laminar. In the free standing PV at low wind, for θ=60° and 45°, i.e. β=30° and 45° respectively, and according to the Gr_c criterion the transition to turbulent is calculated at x=2.07m and x=0.68m, respectively. The latter is smaller than L and that implies transition to turbulent at β=45°. Therefore, $h_{c,b}$ takes higher values than in the smaller β. Similar analysis must be followed for the front side using the proper Gr_c. This is the source of the high dispersion of T_{pv} measured values in low v_w as shown in [17].

3.3 The $h_{c,f}$ and $h_{c,b}$ rate of change vs inclination, β, and temperature, T

3.3a The rate of change of $h_{c,b}$ vs β, $\partial h_{c,b}/\partial\beta$

At natural convection, $\partial h_{c,b}/\partial\beta$ was estimated using eq.(10) [73]:

$$Nu = 0.48\left(\frac{(1+cos\theta)}{2}\right)Gr^{1/4} \quad \text{or equivalently} \quad h_{c,b} = 0.48\left(\frac{k}{L}\right)\left(\frac{1+\cos\theta}{2}\right)Gr^{1/4} \tag{10}$$

For θ=75º or β=15º, L=1.33m, and air conductivity at boundary layer temperature 40º, k=28mW/mK, eq.(10) gives $\partial h_{c,b}/\partial\theta$= -0.94W/m^{2}K/rad. For a change δθ=10^0,that is, 0.1744rad, $\delta h_{c,b}$ is calculated equal to -0.16 W/m^{2}K which is just the value obtained in [69]. This rate increases slowly with Gr. As calculated, $\partial_{c,b}/\partial\theta$ changes linearly from (-3/π)W/m^{2}K/rad, at ΔT=T_{pv}-T_o=10ºC, to -4/π at ΔT=30ºC, and -5/π, at ΔT=50ºC. The negative sign signifies that $h_{c,b}$ decreases as θ increases, i.e. β decreases.

The corresponding values for $\partial h_{c,f}/\partial\theta$ are: 0, for 60º<θ<90º; that is, $h_{c,f}$ is constant in that range. For 30º<θ<60º, or 30º<β<60º, $\partial h_{c,f}/\partial\theta$ =+0.2W/m^{2}K/rad, while for 0º<θ<30º or 60º<β<90º, $\partial h_{c,f}/\partial\theta$ =+0.5W/m^{2}K/rad for ΔT=10ºC. In average, its value is +0.8W/m^{2}K/rad for ΔT=30ºC, and +1.0W/m^{2}K/rad for ΔT=50ºC. The positive sign signifies that $h_{c,f}$ increases as θ increases.

3.3b The $h_{c,b}$ and $h_{c,f}$ rate of change vs T

$\partial h_{c,f}/\partial T$, is estimated around 0.050W/m^{2}K per K for all inclinations, while the average values of $\partial h_{c,b}/\partial T$ are: 0.055, 0.053 and 0.050W/m^{2}K per K for inclinations β=30^0,60^0,90^0, respectively.

3.4 The thermal radiation exchange rates between both PV sides with their environment

To handle the net thermal radiation exchanged between the PV front and back side with sky and ground using a similar expression to the heat convection it is necessary to linearize it. This process introduces the coefficients, $h_{r,f}$ and $h_{r,b}$. In the $h_{r,f}$ and $h_{r,b}$ expressions the following parameters appear: the sky temperature T_{sky}=0.0552(Ta)$^{1.5}$, the Stefan-Boltzmann constant σ equal to 5.67·10^{-8}W/m^{2}K and the view factors, $F_{pv\text{-}sky}$ and $F_{pv\text{-}gr}$, which correspond to the fraction of the radiated heat from the PV surface which reaches the sky, the ground surface or the wall(s) according to the PV-ceiling design and geometry and are determined by eqs.(11a,b) provided that the other surface is much larger than A_{pv}. If this is not the case, more elaborated expressions are developed [70].

$$F_{pv-sky,f} = \frac{(1+\cos(\beta))}{2}, \;\; F_{pv-sky,b} = \frac{(1+\cos(\pi-\beta))}{2} \tag{11a}$$

$$F_{pv-gr,f} = \frac{(1-\cos(\beta))}{2}, \;\; F_{pv-gr,b} = \frac{(1-\cos(\pi-\beta))}{2} \tag{11b}$$

The $h_{r,f(pv\text{-}sky)}$ and $h_{r,f(pv\text{-}gr)}$ are given in [70,73]. For A_{pv}/A_{sky} practically zero and for low β, $F_{pv\text{-}sky}$>>$F_{pv\text{-}gr}$ and then, a simplified formula is provided

$$h_{r,f(pv-sky)} = F_{pv-sky,f}\,\varepsilon_{pv}\sigma\left(T_f^2+T_{sky}^2\right)\left(T_f+T_{sky}\right) \tag{12a}$$

Similarly, for A_{pv}/A_{gr} practically zero, and high inclination, β, $F_{pv\text{-}gr}$>>$F_{pv\text{-}sky}$ and then

$$h_{r,f(pv-gr)} = F_{pv-gr,f}\,\varepsilon_{pv}\sigma\left(T_f^2+T_{gr}^2\right)\left(T_f+T_{gr}\right) \tag{12b}$$

For A_{pv} equal to the surface close and opposite to it, as it is the case of the BIPV, $F_{pv\text{-}plank}$=1 and the coefficient $h_{r,b}$ for the radiated heat exchanged between PV back side and its back cover is given by,

$$h_{r,b(pv-int)} = \frac{\sigma(T_b^2+T_{pl}^2)(T_b+T_{pl})}{\left(\frac{1}{\varepsilon_{pv}}+\frac{1}{\varepsilon_{pl}}-1\right)} \tag{13}$$

ε_{pl} is the emissivity coefficient of the plank opposite the PV back side inside the BIPV and T_{pl} its temperature, in K. The radiative heat exchange rates differ due to the different sky and ground temperatures, T_{sky} and T_{gr}, the view factors of the front and back PV sides which depend on the module inclination β, eqs.(11a),(11b), the geometry of the BIPV configuration and the emissivity coefficients for Tedlar and glass cover. Those were measured ε_b=0.91 and ε_g=0.85 respectively, by using the Surface Optics Corp. ET10 emissometer. The sky, ground and indoor walls/plaster emissivity coefficients were taken equal to ε_{sky}=0.91, ε_{gr} =0.94, ε_{pl}=0.92 [5,18,75,76].

Based on the analysis so far, $h_{c,b}$ in the BIPV was estimated around 2-3W/m^2K compared to 4-6W/m^2K for the $h_{c,f}$ at low v_w for the open air BIPV, PV fixed and sun-tracking configurations. $h_{r,f}$ and $h_{r,b}$ using the above equations were estimated 5±0.5W/m^2K for the above PV configurations. The rates of change of $h_{r,f}$ and $h_{r,b}$ vs β and T are given below.

3.5 $h_{r,f}$ and $h_{r,b}$ dependence on β and T

$h_{r,f}$ increases vs β or decreases vs θ. At horizontal, the view factor $F_{pv\text{-}sky}$ is 1 and the net thermal radiation exchanged is higher as T_{sky} is much lower than T_{gr}=T_a. For β>45^o the thermal radiation exchanged has a strong component between PV front side and ground, while for β<45^o the thermal radiation exchanged between PV and ground is lower than 15% due to the low $F_{pv\text{-}gr}$ where $F_{pv\text{-}gr}$ =(1-cos(β))/2, while the $F_{pv\text{-}sky}$ = (1+cos(β))/2. $h_{r,b}$ is considered the same way.

3.6 The $h_{r,f}$ and $h_{r,b}$ rates of change vs T

The estimated average rate is equal to $\partial h_{r,f}/\partial T$= $\partial h_{r,b}/\partial T$=0.02W/$m^2$K per K for deviation of the T_{pv} from a reference temperature, δT_{pv}= T_{pv}-$T_{pv,ref}$. Note $T_{pv,ref}$ is defined as the T_{pv} at SOC.

3.7 The rate of change $\partial h_{r,f}/\partial\beta$

It is negligible for 60^o<θ<90^o or 0^0<β<30^o. For 30^o<β<60^o, $\partial_{r,f}/\partial\beta$ was estimated around +0.12W/m^2K per rad. For 60^o<β< 90^o its value is +0.22W/m^2K per rad. The sign changes when $\partial h_{r,f}/\partial\theta$ is used.

3.8 The rate of change $\partial h_{r,b}/\partial\beta$

In the PV fixed and the sun-tracking system the rate of change is negligible for 0^o<β<30^o while, for 30^o<β<60^o it was estimated equal to -0.12W/m^2K/rad and for 60^o<β<90^o it was estimated equal to -0.20W/m^2K/rad. Its sign is opposite to the one of $\partial h_{r,f}/\partial\beta$.

3.9 The inclination effect at natural and air forced flow.

The $h_{c,f}$ and $h_{c,b}$ depend on β and T and strongly on v_w. Their values increase faster compared to $h_{r,f}$ and $h_{r,b}$ which are loosely β and T dependent. For moderate to high wind speed $h_{c,f}$ gets higher than $h_{r,f}$ and hence its β dependence gets much weaker [77]. The issues highlighted in this Section explain the pattern of scattered values in the *f* profile for low v_w shown in [17]. Using the above mentioned rates of change and the theoretical analysis in [55-66,68-69], the sum of $h_{c,f}$, $h_{c,b}$, $h_{r,f}$ and $h_{r,b}$ which equals U_{pv} is calculated.

4. Theoretical elaboration of the proposed model to predict T_{pv}, *f* and P_m

The model proposed is based on 3 key issues:

1. The determination of an implicit function *f* shown below:

$$T_{pv} = T_a + f\big(v_w, \eta_{pv}(T_a, T_{pv}, I_T, v_w), U_{pv}(T_{pv}, I_T, v_{w,}\beta)\big) I_T \tag{14}$$

2. The development of an empirical expression $f(v_w)$ to reflect the contribution of v_w on *f*. That was done through a regression analysis of the PV sun-tracking monitored data I_T, T_a, T_{pv} and v_w

3. The development of a set of mathematical expressions for the accurate determination of *f* taking into consideration the PV module age, the PV module efficiency, the field conditions v_w, T_a, I_T, the (BI)PV configuration and the deviations of $\eta_{pv}(T_a, T_{pv}, I_T, v_w)$ and $U_{pv}(T_{pv}, I_T, v_w, \beta)$ from their corresponding values at SOC.

The combination of the EBE for a PV module at steady state [7] with eq.(14) gives,

$$f = \frac{1-\eta_{pv}}{U_f+U_b} - \frac{U_f}{(U_f+U_b)I_T}\Delta T_{f-b} \qquad \text{where } \Delta T_{f-b} = T_f - T_b \tag{15}$$

The first term in eq.(15) is considered as a zero approach to *f*, f_o, where:

$$f_o = \frac{1-\eta_{pv}}{U_f+U_b} \qquad \text{and hence,} \tag{16}$$

$$f = f_o - \frac{U_f}{(U_f+U_b)I_T}\Delta T_{f-b} \tag{17}$$

ΔT_{f-b} was experimentally measured between 0 and -3°C. The value depends on the PV mounting mode, the cell material, construction and the v_w strength and direction. U_f and U_b may be estimated through iterations [21]. However, this would not lead to a compact T_{pv} prediction tool as sought for here. At low v_w or in wind protected areas such as the BIPV back side with the modules integrated within the roof, U_f and U_b according to Section 3 take values within [10-13]W/m²K and [7-10]W/m²K, respectively. Hence, U_f+U_b=[17-23]W/m^{2}K. Using these values for this BIPV mode, eq.(17) gives f in the range of [0.035, 0.050]m^{2}K/W. Similarly, the same range of f values holds for the PV fixed and sun-tracking at low v_w, whereas as v_w increases, >3m/s, U_f and U_b increase to about 20 ± 2W/m^{2}K each, and thus f reduces to within [0.020 - 0.025]m^{2}K/W, as shown in Fig.3. The v_w effect on f is strong, while the effect of the correction term in eqs.(17,18) due to T_{pv} may reach up to [7.5% -10%].

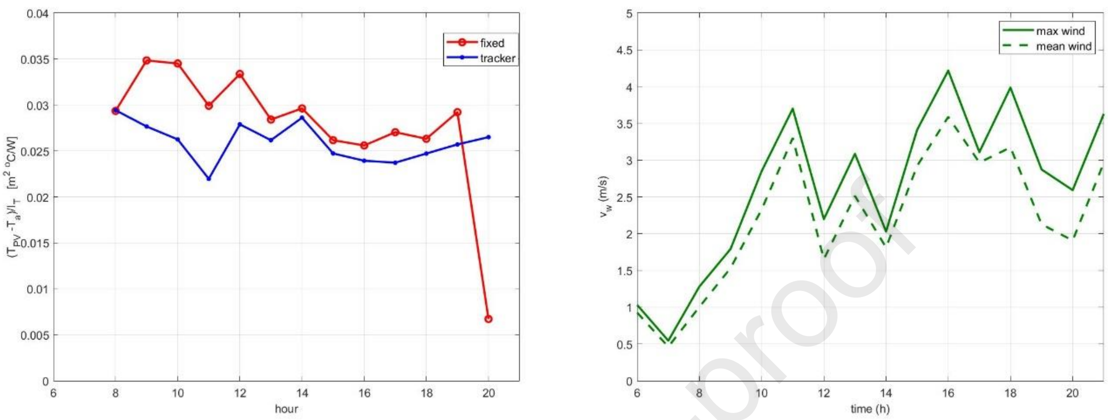

(a) (b)

Fig.3. The profiles of (a) f and (b) v_w during a day in July for the sun-tracking and fixed PV systems. The effect of v_w on f is obvious and ranges from 0.038 m^{2}K/W when v_w is low to 0.022-0.025 m^{2}K/W for higher v_w.

To build the new model, f may be expressed instead by eq.(18) as a product of a function of v_w the dominant part and a weaker function of η_{pv} and $(U_f + U_b)=U_{pv}$, both dependent on T_{pv}, I_T, , v_w and β:

$$f = f(v_w) f\big(\eta_{pv}(T_a, T_{pv}, I_T, v_w), U_{pv}(T_{pv}, I_T, v_w, \beta)\big) \tag{18}$$

A Taylor series expansion of the f function at $v=v_w$, and estimation of its partial derivatives for η_{pv} and U_{pv} around the SOC values provide a general expression for f in the form of eq.(19):

$$f = f(v_w)\left(1-\frac{\delta\eta_{pv}}{1-\eta_{pv,SOC}}\right)\left(1-\frac{\delta U_{pv}}{U_{pv,SOC}}\right) \tag{19}$$

Therefore, the compact formula to predict ***f* for natural flow** or v_w<1.5m/s is:

$$f = f(v_w)\left(1-\frac{\left(\left(\frac{\partial\eta_{pv}}{\partial T_{pv}}\right)\delta T_{pv}+\left(\frac{\partial\eta_{pv}}{\partial I_T}\right)\delta I_T\right)}{(1-\eta_{pv,SOC})}\right)\left(1-\frac{\left(\frac{\partial U_f}{\partial T_{pv}}\right)\delta T_{pv}+\left(\frac{\partial U_b}{\partial T_{pv}}\right)\delta T_{pv}+\left(\frac{\partial U_f}{\partial\beta}\right)\delta\beta+\left(\frac{\partial U_b}{\partial\beta}\right)\delta\beta}{U_{pv,SOC}}\right) \tag{20}$$

Regression analysis was applied on the 1st year recorded T_b, v_w, I_T, T_a data from the sun-tracking PV. A rational function, eq.(21), was fitted because it complies with the weak v_w dependence of η_{pv} in the nominator in eq.(19) and the strong dependence of U_{pv} on v_w in the denominator. The parameters in eq.(21) correspond to the SOC values of T_a, I_T, used as a reference for the *f* corrections due to environmental fluctuations. In this analysis, it holds: $\delta T_a = T_a - 20^oC$, $\delta I_T = I_T - 800W/m^2$, and $\delta\beta = \beta - 38^o$.

$$f(v_w) = \frac{a + b v_w}{1 + c v_w + d v_w^2} \tag{21}$$

where *a= 0.0375, b=0.0081, c=0.2653, d=0.0492*

The analysis outlined in the Appendix is used to determine the quantities and parameters in eq.(20). For this, eq.(21) and the expressions (A.1)-(A.6) in the Appendix are used to consider the effect of $\delta\eta_{pv}(T_{pv},I_T)$ and $\delta U_{pv}(T_{pv},\beta)$.When heat transfer from the module to the environment is due to air forced flow the factor $\delta U_{pv}/U_{pv,SOC}$) gets negligible because of the weak dependence of U_{pv} on T_{pv} and β compared to natural heat flow. Then, eq.(20) is reduced to eq.(22) which is the compact formula to predict ***f* for forced convection** or $v_w \geq 1.5m/s$:

$$f = f(v_w)\left(1 - \frac{\left(\frac{\vartheta\eta_{pv}}{\vartheta T_{pv}}\right)\delta T_{pv} + \left(\frac{\partial\eta_{pv}}{\partial I_T}\right)\delta I_T}{1 - \eta_{pv,SOC}}\right) \tag{22}$$

Accurate *f* values are estimated from eqs.(20,22) for natural or forced flow, respectively, by setting initially $(\vartheta\eta_{pv}/\vartheta I_T)\delta I_T=0$ and neglecting the effect of δU_{pv} in eq.(20). This approximate *f* value is then substituted into eq.(A.5) to estimate $(\vartheta\eta_{pv}/\vartheta I_T)\delta I_T$. Then *f* is re-estimated from eq.(20) or eq.(22).. Eqs.(A.1)-(A.6) provide the expressions to estimate the parameters required in eq.(22). Under air forced flow where the terms $\vartheta U_f/\vartheta T_{pv}$, $\vartheta U_b/\vartheta T_{pv}$, $\vartheta U_f/\vartheta\beta$, $\vartheta U_b/\vartheta\beta$ are negligible.

For natural air flow *f* is obtained by eq.(20). In this case, the U_{pv} at SOC is denoted as $U_{pv,SOC}$. $\eta_{pv,SOC}$ is determined from eq.(A.1) while eq.(21) for v_w=0 m/s gives $f(v_w=0)$=0.0347. $U_{pv,SOC}$ is then estimated from eq.(23).

$$U_{pv,SOC} = \frac{(1 - \eta_{pv,SOC})}{f(v_w = 0)} \tag{23}$$

The average rates of change for U_{pv} with respect to T_{pv} and β in eq.(20) are provided by eqs.(A.6a)-(A.6d). Note, for a PV module with $\delta\beta=10^o$ and $\delta T_{pv}=T_{pv}-T_{pv,SOC}=10^oC$, with reference to ($\beta=\varphi$, *and* $T_{pv,SOC}=20^oC+f(v_w=0)\cdot 800W/m^2$), and for a $U_{pv,SOC}$ value at the average environmental conditions, $U_{pv,SOC}$=23.9Wm^{2}K, determined from eq.(23), the contribution of δU_{pv} due to $\delta\beta$ and δT_{pv} variations is estimated +5-6%, while, the corresponding of $\delta\eta_{pv}$ is -12%.

Additional correction terms are introduced in the *f* and T_{pv} prediction, to cater for the PV cell type, and the age of the module under testing. The $f(v_w)$, eq.(21), was derived for a pc-Si with nominal η_{pv}=0.121. Its efficiency at STC after 8 years of operation was estimated equal to $\eta_{pv,STC}$=0.11 taking into account 9% degradation overall. Eq. (A.1) is used to estimate the efficiency at SOC, $\eta_{pv,SOC}$. To generalize the formula for any PV module tested of a given efficiency at SOC denoted as $\eta_{pv,n}$ an additional correction factor is introduced in eqs.(20,22) which has the form, $(1- \delta\eta_{tec}/(1-\eta_{pv,SOC}))$. $\delta\eta_{tec} = \eta_{pv,n} - \eta_{pv,SOC}$, where $\eta_{pv,SOC}$=0.095 and $\eta_{pv,n}$ is the efficiency of the new type of module at SOC. A third correction term is introduced for the natural degradation of the module and provides the decrease $\delta\eta_{ag}$ due to aging with reference to the age, 8 years, of the pc-Si module used to develop the model.

$$\delta\eta_{ag} = -\eta_{pv,SOC} \cdot (0.8\% \cdot N - 9\%) \tag{24}$$

where N are the years in operation of the PV module to be studied.

The holistic f prediction formula which considers field conditions, cell type, and age takes the form

$$f = f(v_w)\left(1 - \frac{\delta\eta_{pv}}{(1-\eta_{pv,SOC})}\right)\left(1 - \frac{\delta U_{pv}}{U_{pv,SOC}}\right)\left(1 - \frac{\delta\eta_{ag}}{(1-\eta_{pv,SOC})}\right)\left(1 - \frac{\delta\eta_{tec}}{(1-\eta_{pv,SOC})}\right) \tag{25}$$

The $f(v_w)$ expression is the same for any PV cell technology as it echoes the effect of v_w on U_f and U_b whose values for any planar PV cell technology are practically the same.

Scaling factor SF for BIPV configurations

The proposed expressions for f and T_{pv} prediction hold for both free-standing PV and BIPV configurations, however for the latter case, a scale factor, SF, is required to adapt this model for the BIPV where v_w has a negligible effect on its PV back side. Note that this factor is not required for BAPV configurations. For the BIPV case f in eqs.(20,22) is multiplied with SF, which takes into account the U_b decrease in the BIPV compared to the open air PV. U_f for the free environment and U_b for both free and indoor conditions were estimated in the beginning of Section 4. SF is derived by substituting into eq.(17) the U_f and U_b values once for indoor conditions and then for free. Their ratio gave ***SF=1.35* for forced flow** with $v_w \geq 1.5$m/s and ***SF=1.18* for natural flow** or $v_w < 1.5$m/s.

P_m may then be predicted at any hour h from the predicted T_{pv} and the I_T through eq.(26a):

$$P_m = P'_{m,STC} \cdot [1 + \gamma(T_{PV} - 25^oC) + \delta \cdot \ln(I_T/1000)] \cdot (I_T/1000) \tag{26a}$$

$$P'_{m,STC} = P_{m,STC}(1 - r_{ageing}) \tag{26b}$$

$$P_{m,sys} = P_m(1 - \varepsilon_{losses}) \tag{26c}$$

where γ is the temperature coefficient for P_m with value in the region [-0.4, -0.5] %/ºC and δ the solar irradiance coefficient with value 0.085 for sc-Si and 0.11 for pc-Si modules [79]. $P'_{m,STC}$ the PV peak power at STC at the current state of the system considering PV degradation due to ageing. The overall percentage due to ageing is denoted here as r_{ageing}. P_m represents the array output at operating conditions and $P_{m,sys}$ the final power output of the system with ε_{losses} the percentage of additional power conditioning losses at system level.

5. Results and Analysis

The theoretical analysis in Section 4 shows that the factors β, v_w, T_{pv} and I_T affect explicitly and/or implicitly f, T_{pv} and P_m. The proposed model succeeded to integrate the overall effect of those factors into one formula, eqs.(14,20,22,25) and to addresses the impact of those parameters through correction terms. The predicted by this model T_{pv} for free-standing PV and BIPV modes is compared with the measured values and also, with those predicted by other known models as shown in the following sections.

5.1 T_{pv} prediction results for the PV sun-tracking configuration and model validation

For the model validation, f and T_{pv} for the sun-tracking PV system, operating at a wide range of I_T, v_w,T_α and β, were predicted using eqs.(20-25). The predicted T_{pv} values were compared with measured ones, using the 2nd year monitoring data from the sun-tracking system and are presented in Fig.4. The proposed model exhibits an excellent prediction capacity with slope equal to 1.004 with R^2=0.9183. Extensive comparison was carried out comparing measured T_{pv} with predicted values by 3 other models proposed in [11,31,36]. For the model in [36] the predicted vs measured T_{pv} has slope 0.8658 with R^2=0.8992, see Fig.5. For the model in [11], the slope is 0.871 with R^2=0.8851, Fig.6, and for the model in [31] the slope is 0.8396 with R^2=0.8572, see Fig.7. The linear fit in Figs.5-7 discloses that the 3 models underestimate T_{pv} at high values, which occur at high I_T and low v_w. On the other hand, the proposed model shows an excellent behavior with the linear fit nearly matching the diagonal across the entire spectrum of I_T and v_w.

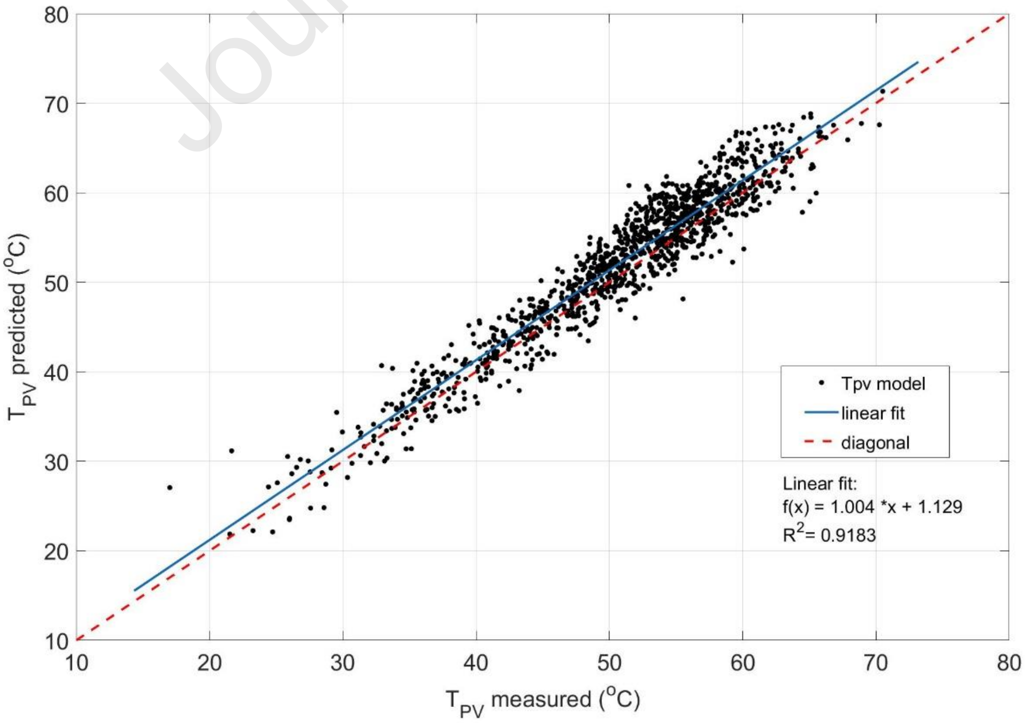

Fig.4. Validation of the proposed model. Predicted T_{pv} vs measured values using the 2nd year monitored data from the sun-tracking PV system.

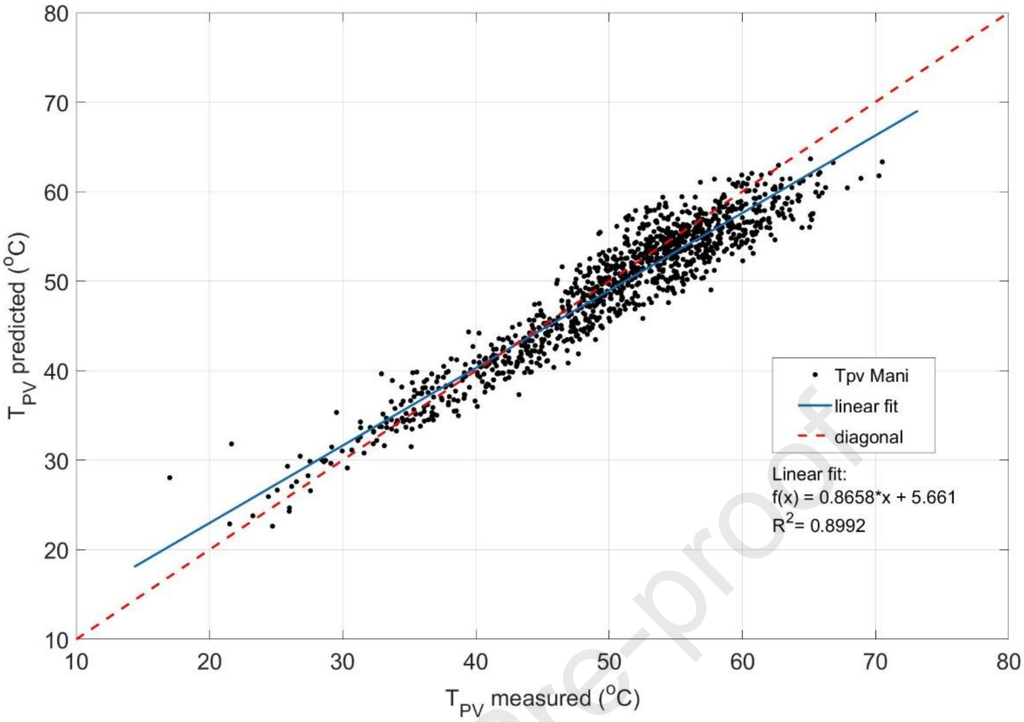

Fig.5. Predicted T_{pv} applying Mani's model [36] vs measured values using the 2nd year monitored data from the sun-tracking PV system.

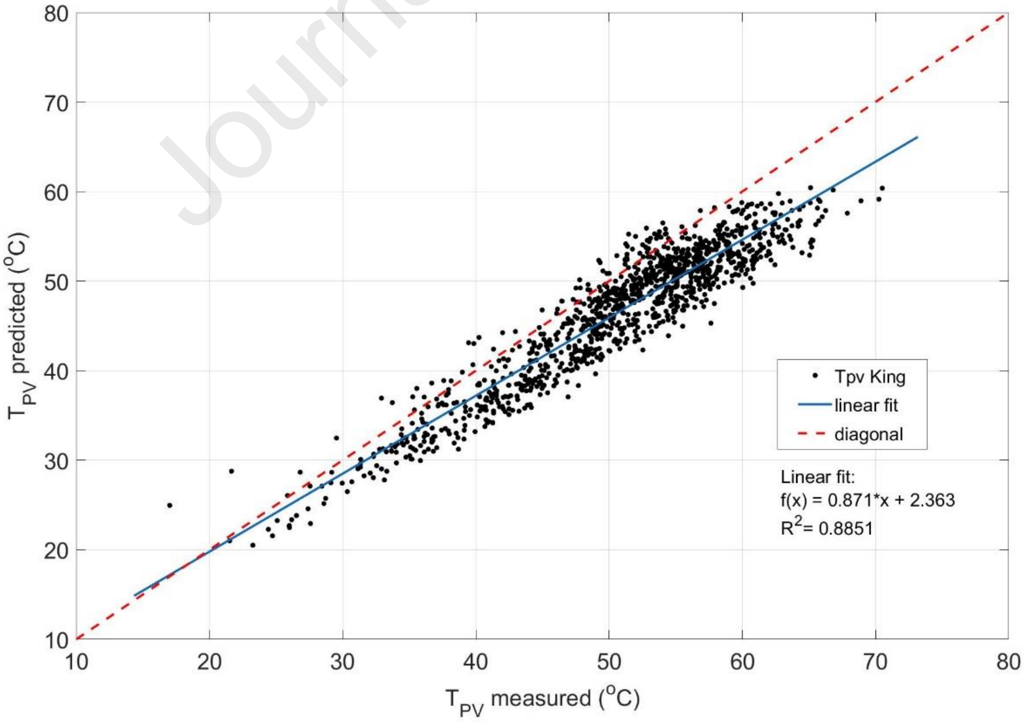

Fig.6. Predicted T_{pv} applying King's model [11] vs measured values using the 2nd year monitored data from the sun-tracking PV system.

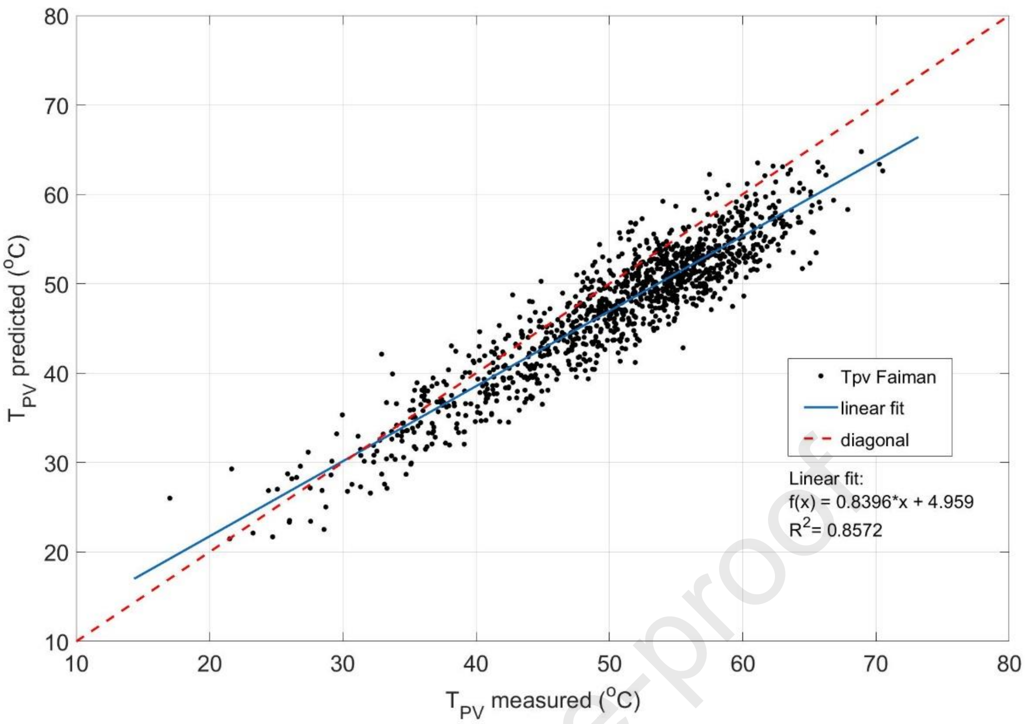

Fig.7. Predicted T_{pv} applying Faiman's model [31] vs measured values using the 2nd year monitored data from the sun-tracking PV system.

P_m was predicted by eqs.(26a-26c) using the T_{pv} predicted by this model, and compared with the experimentally determined P_m values from the sun-tracking PV system using the monitoring data of the 2nd year. For the P_m prediction the PV module power degradation was determined 10% for the 9th year of operation, while 5% power conditioning losses were considered for the PV system final power output. The predicted vs measured P_m is displayed in Fig.8, showing excellent results with slope 1.005 and R^2=0.8579. This performance is superior to the predictions by the other 3 models and similar to the predictions by the dynamic electro-thermal PV temperature simulation model, as shown in [21].

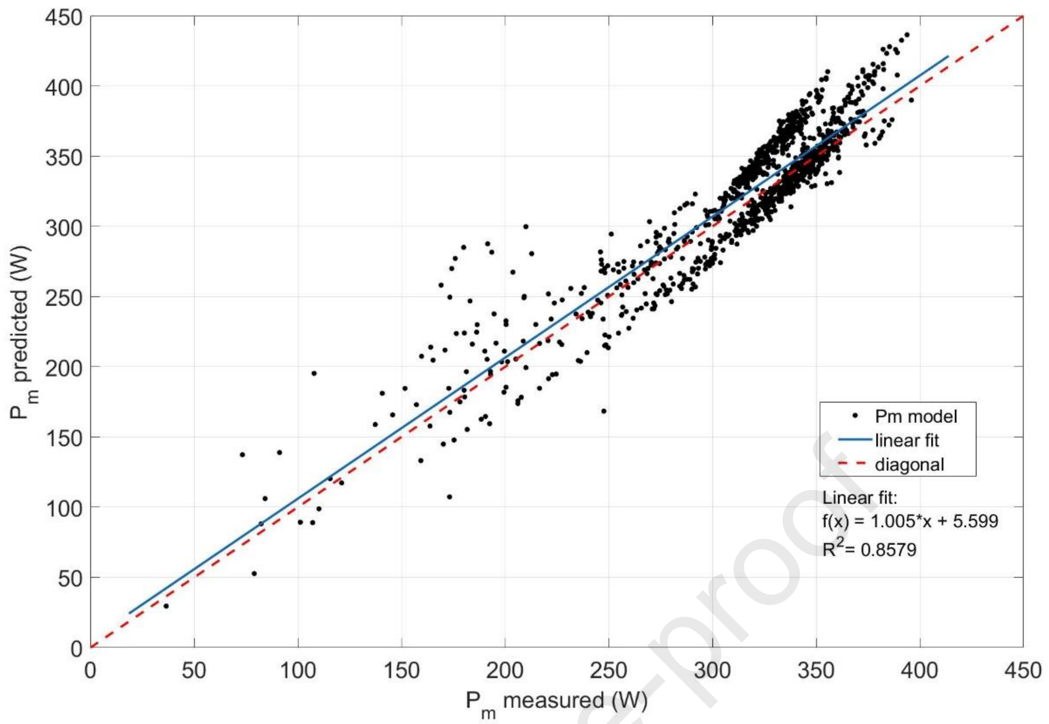

Fig.8. P_m predicted by this model vs experimentally determined values using the 2nd year monitored data from the PV sun-tracking PV system.

5.2. T_{pv} prediction results for the BIPV configuration and model validation

T_{pv} for the BIPV of Fig.2(c) was predicted with this model using eqs.(20) for v_w<1.5m/s and eq.(22) for v_w≥1.5m/s multiplying the predicted *f* values with SF=1.18 and 1.35 respectively, according to the analysis outlined in Section 4. Fig.9 shows the predicted T_{pv} profiles by the proposed model and by the 3 other models vs the measured T_{pv} profiles at the PV back surface of the BIPV system during 5 clear-sky consecutive days in June, with 1 min time interval. The v_w and I_T profiles are plotted in the bottom subplots, with wind speed ranging from 0 to 7.9m/s. Fig.10 shows the same comparison for 3 days in April with partly cloudy sky and wind speed ranging from 0 to 8.2m/s. The T_{pv} predicted by this model lies very close to the measured T_{pv} profile data, and exhibits superior performance for both clear sky and partly cloudy days and across the large range of wind speeds 0-8.2m/s, when compared to the other well-known models [11,31,36] which exhibit large deviations from the measured values. The effect of v_w on the predicted and measured profiles is obvious and conforms with the analysis in Section 4.

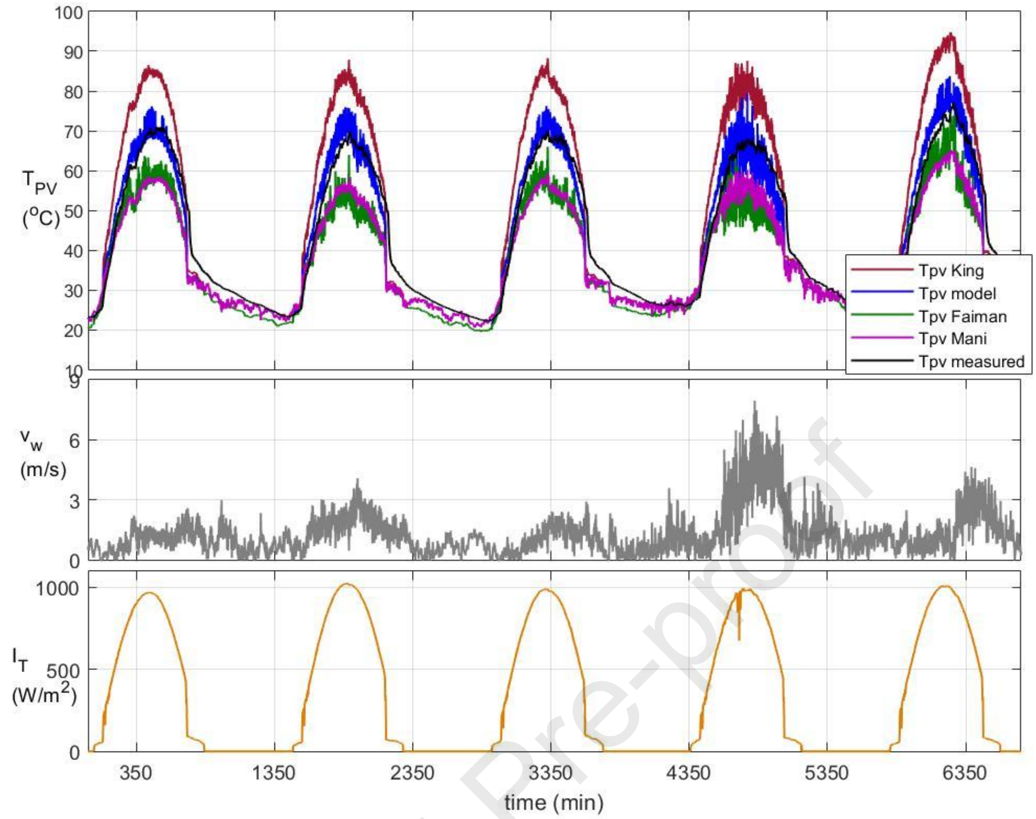

Fig.9. Predicted T_{pv} profiles by this model and by the 3 other models in [11,31,36] vs measured ones at the BIPV back surface during 5 consecutive days in June with 1 min time interval. I_T and v_w are plotted in the bottom subplots.

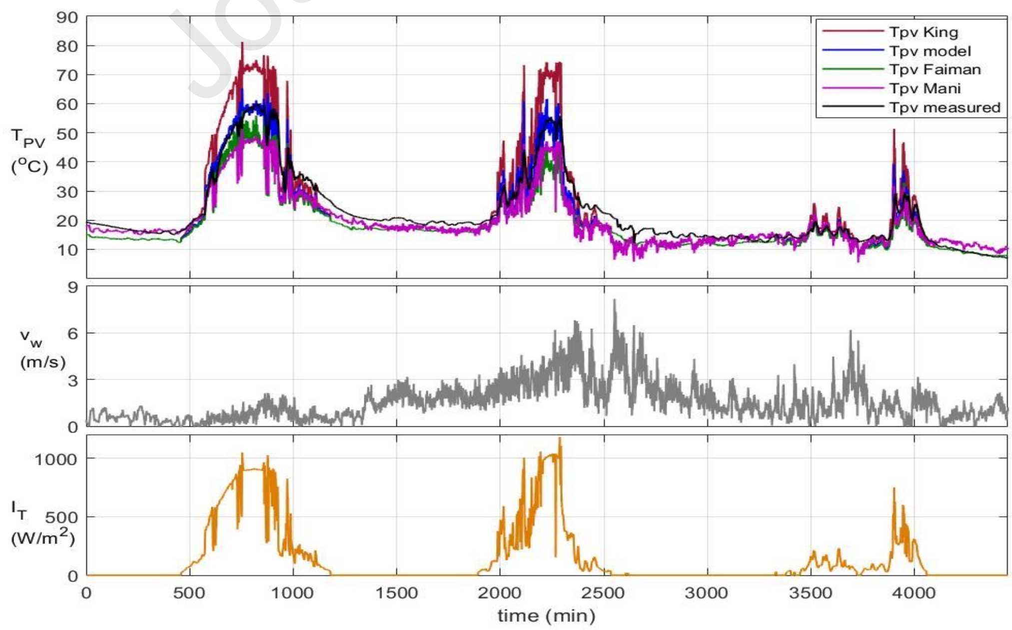

Fig.10. Same as in Fig.9 for 3 consecutive days in April.

The predictive capacity of this model for the BIPV case is shown in Fig.11, where the predicted vs measured T_{pv} for the period April-May-June is displayed. The linear fit has slope 1.027 with R^2=0.9184, very close to the diagonal, exhibiting excellent model performance. For comparison the predicted T_{pv} by the models in [36,11,31] vs the measured BIPV data for the same period are shown in Figs.12-14 respectively. The slope of the fitted line show that the models [31,36] underestimate T_{pv} while the model [11] overestimates it. This comparison highlights the high predictive capacity of the proposed model which is attributed to this novel approach integrating most of the environmental parameters which affect T_{pv} and η_{pv}, and the latter's deviation from the SOC values, the rates of change of U_{pv} vs T_{pv} and β, the PV mounting through SF, the module technology through the η_{pv} and the operational condition of the module through the number of years of operation and degradation rate.

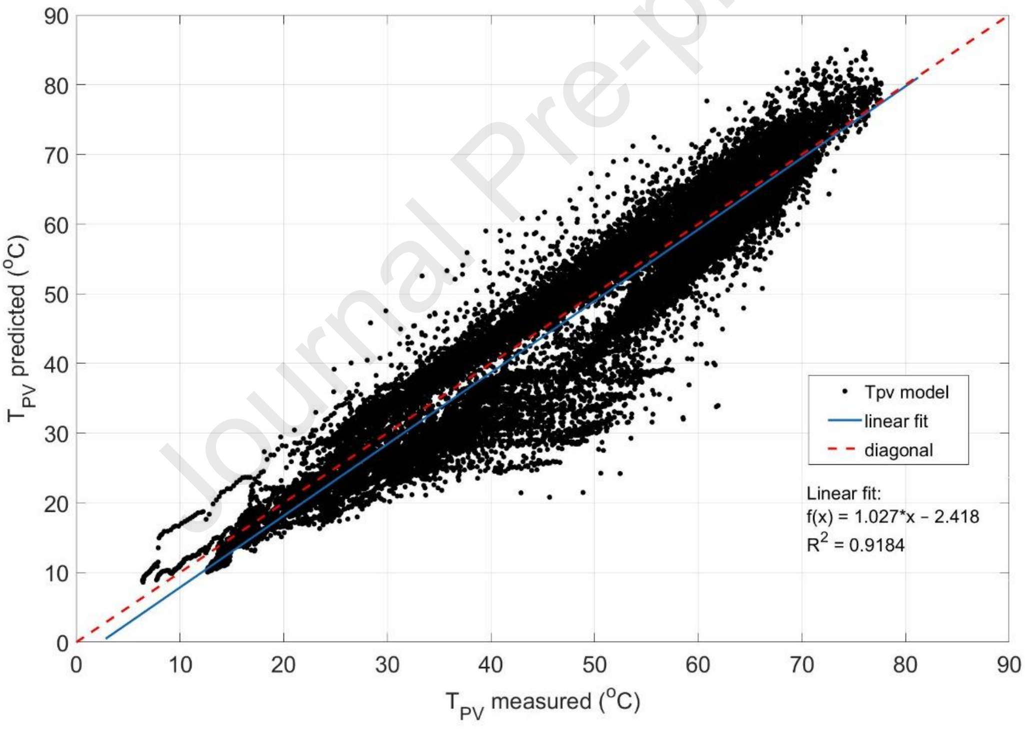

Fig.11. Predicted T_{pv} by this model vs measured values from the BIPV system monitored across the period April-May-June, with 1 min interval.

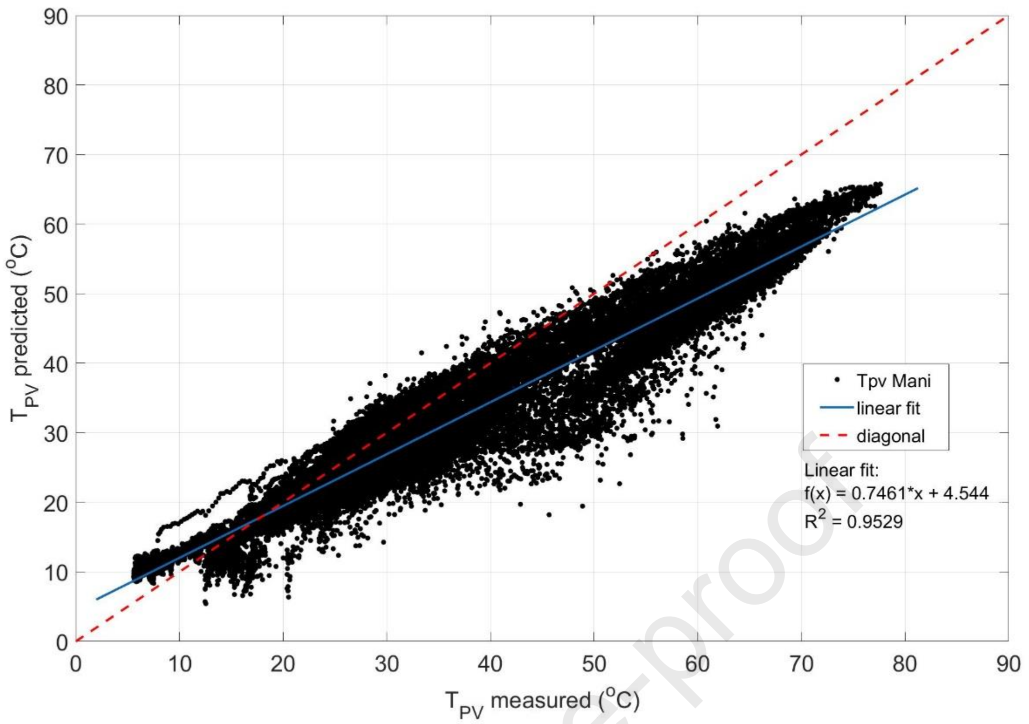

Fig.12. Predicted T_{pv} applying Mani's model [36] vs measured values from the BIPV system monitored across the period April-May-June, with 1 min interval.

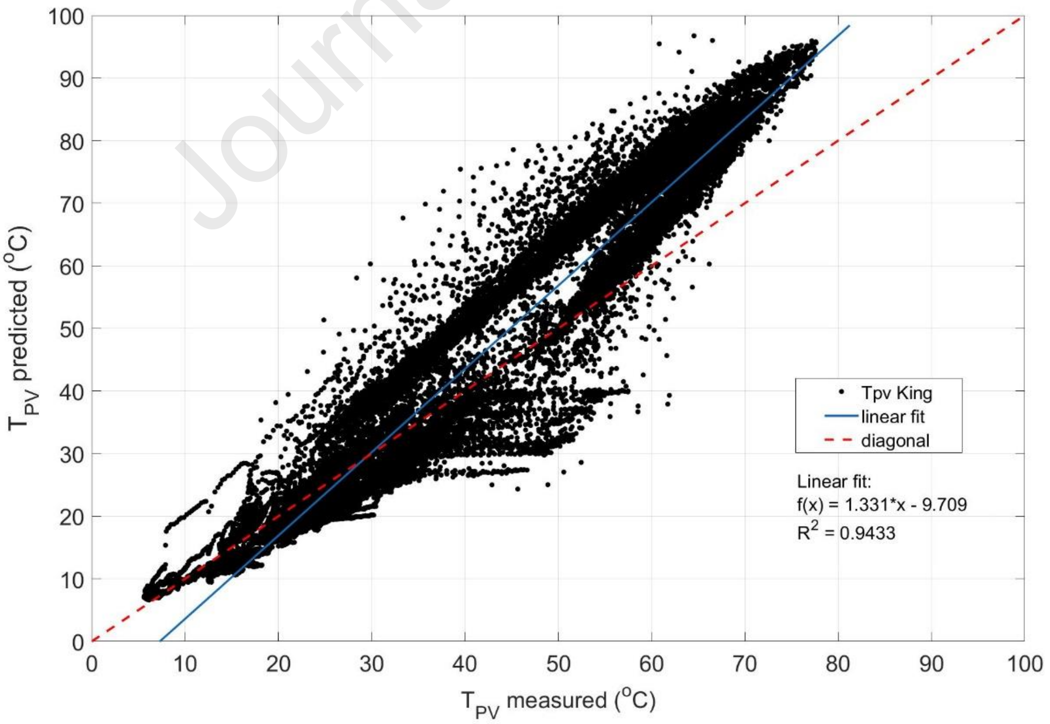

Fig.13. Predicted T_{pv} applying King's model [11] vs measured values from the BIPV system monitored across the period April-May-June, with 1 min interval.

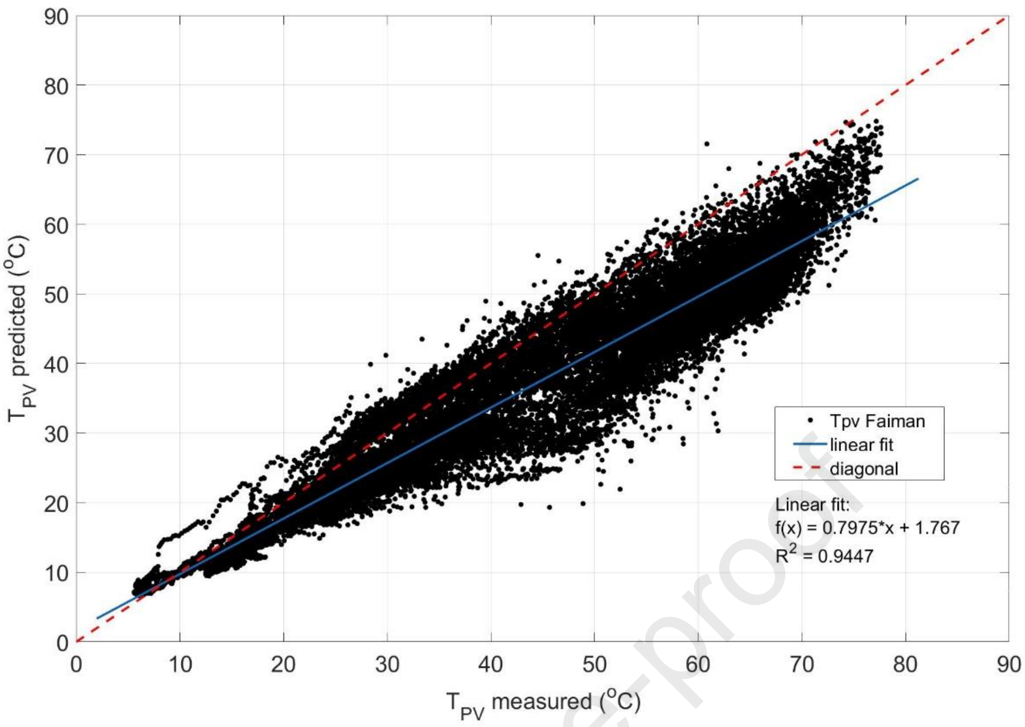

Fig.14. Predicted T_{pv} applying Faiman's model [31] vs measured values from the BIPV system monitored across the period April-May-June, with 1 min interval.

5.3 Proposed model applied to other BIPV configurations

The model's predictive performance is further evaluated against experimental data reported in other studies for different BIPV types, mounting configurations and conditions as shown in Table 2. The BIPV in NREL [59] includes two mounting configurations, one with the PV modules directly mounted on the roof and the other with counter-battens mount, which allows air flow at the back of the modules. The model of eq.(25) is evaluated with the experimental data of the above study for both mounting configurations. The scaling factor SF=1.35 (forced flow) is applied for the BIPV with direct-mount while no scaling factor (SF=1) is applied for the counter-battens mount because it allows air to flow free at the back of the module. The predicted values are within ±1°C from the measured values for both mounting configurations and both set of conditions as shown in Table 2. Since the conditions reported in [59] were for v_w>2m/s, then according to the analysis in Section 4, the 3rd term $\left(1 - \delta U_{pv}/U_{pv,SOC}\right)$ in eq.(25) is dropped as this term accounts only for natural flow (v_w<1.5m/s). The performance of the model for natural convection which now includes this term is shown in comparison to the measured data for BIPV in the façade and roof of [46,54] for the conditions of no wind. The T_{pv} predictions by eq.(25) are within ±1.5°C (Table 2). In this case the scaling factor applied is SF=1.18 corresponding to natural flow and v_w<1.5m/s. In the cases of fully integrated PV with small airgap and direct mount the

SF is applied, whereas for partly integrated PV the SF in not applied according to Section 4. For the conditions of higher wind speed in the aforementioned mounting configurations the T_{pv} predictions by eq.(25) are within ±3^{o}C from the measured values. On the other hand, studies [46,54] include their own predictions using the SNL [11] and NOCT models and refining the Ross coefficient [27], which exhibit deviations from measured values as large as ±11^{o}C. All these illustrate the high accuracy and wide applicability of the model proposed which shows excellent performance compared against the experimental data from BIPVs in different locations, mounting configurations, PV technology and age of operation, similar scale [46,54] to the BIPV of the current study or larger scale [59] and across a variety of weather conditions. The applicability of the SF is illustrated for BIPV/BAPV of different mounting configurations in Table 2.

Table 2: T_{pv} model performance with experimental data of other studies for various BIPV configurations.

Reference Study	BIPV type	Prediction Approach	Conditions	Measured T_{pv} in the reference study (^{o}C)	Predicted T_{pv} in the reference study (^{o}C)	Predicted T_{pv} by eq.(25) (^{o}C)
Muller et al. [59]	pc-Si modules mounted on the roof, slope 15^o, in direct-mount and counter-battens mount	Measured data, average values	T_a=28.6 ^{o}C I_T=996.8 W/m^2 v_w=2.49 m/s	67.4 (direct-mount)	N/A	68.4 (with SF=1.35)
				59.0 (counter-battens)		58.1 (SF=1)
			T_a=27.5 ^{o}C I_T =577.7 W/m^2 v_w=2.07 m/s	48.9 (direct-mount)		50.0 (with SF=1.35)
				44.0 (counter-battens)		44.2 (SF=1)
Toledo et al. [54]	c-Si modules integrated on the South Façade	Refining empirical coefficient of Ross [27] and SNL model [11]	@12:00 T_a=38.4 ^{o}C I_T=540 W/m^2 v_w not reported (v_w=0)	60.5	54.1 (Ross) 58.8 (SNL)	60.7

D’Orazio et al. [46]	c-Si modules mounted on roof, slope 17°, fully integrated with small air gap, direct mount and partly integrated PV (large air gap)	Predicted through NOCT and SNL models	@12:30 T_a=34 °C I_T=945 W/m^2 no wind,v_w=0	76 (fully integrated with small air gap)	65 (NOCT) 80 (SNL)	74.6 (SF=1.18)
			@13:30 T_a=27°C I_T=940 W/m^2 v_w=4.15m/s	59.5 (direct-mount)	57 (NOCT) 69 (SNL)	56.6 (SF=1.35)
			@13:30 T_a=27°C I_T=940 W/m^2 v_w=4.15m/s	47 (partly-integrated)	57 (NOCT) 54 (SNL)	48.9 (SF=1)

6. Discussion

The proposed model (eq.(25)) is a function of environmental conditions T_a, I_T, v_w and interrelated module parameters η_{pv}, T_{pv}, mounting related parameters β, U_{pv} and the operational condition of the module determined by its natural degradation based on the number of years of operation. It is expressed as a compact formula making it robust in predicting PV temperature both for free-standing PV and BAPV with large air gap behind the PV modules, as well as BIPV designs for roofs or facades, or BIPV/T when multiplied appropriately with SF depending on a natural or forced flow. SF is applied for the BIPV types with insulated back or small airgap behind the module considering full PV integration into the building structure. The SF is not applied for cases of BAPV where the PV modules are adapted or partly integrated into the building forming a large air gap behind the modules allowing the circulation of external air.

In the previous section, the model was shown to have higher predictive capacity than the widely used and universally accepted formulas [11, 31, 36] and NOCT model along with refined Ross coefficient [27,54] and it is shown to have excellent performance with different BIPV types, mounting configurations, PV technologies and at different locations. The model has not incorporated the effect of humidity and water impact which are critical parameters in floating PV systems and therefore is more appropriate for low to medium humidity conditions in in-land PV systems. Exogenous parameters such as shading from nearby buildings/structures may affect the predictive performance in a similar way to other T_{PV} models. When the solar irradiance is measured locally on the BIPV and the shading impacts on the entire PV array then its effect is reflected directly in the value of solar irradiance which appears reduced and the model predicts T_{pv} and P_m at the new irradiance level. However, localised shading effects, when the module is only partly shaded, would be a challenging issue and is not incorporated within the generalised model –this is outside the scope of the present study.

The effect of PV ageing is taken into account through the term $\left(1 - \delta\eta_{ag}/\left(1 - \eta_{pv,SOC}\right)\right)$ in eq.(25) considering natural degradation of the modules and provides the difference in the efficiency $\delta\eta_{ag} = -\eta_{pv,SOC} \cdot (0.8\% \cdot N - 9\%)$ due to aging of the module under study with reference to the degradation (9%) of the pc-Si modules used to develop the model. In brand new PV installations this term will be used with N=1 leading to an increase in $\delta\eta_{ag}$ compared to the reference module used in the study. The higher the degradation the higher the value of the term $\left(1 - \delta\eta_{ag}/\left(1 - \eta_{pv,SOC}\right)\right)$ and the higher the resulting value of *f* in eq.(25) which illustrates the increase in the predicted T_{pv} due to ageing. Some PV manufacturers nowadays guarantee a smaller degradation rate than 0.8% per year and so the term above could be used with a smaller rate if that is available for the PV installation to be applied. The above term accounts for natural degradation of PV modules and the effect of more severe localized degradation phenomena on T_{pv} is not included here but can be largely accounted for if the term 0.8%N in the above is replaced by the measured degradation of the PV modules to be studied after characterization tests are performed.

An analysis of the predicted (T_{pv}) vs measured (T_m) values shows that the relative error of the prediction for the free-standing system, based on the results presented in Fig. 4, is: $(T_{PV} - T_m)/T_m = 0.004 + 1.129/T_m$. This, for PV operating temperatures around the NOCT and specifically T_m=50ºC gives a relative error 2.6% and for temperatures in the higher range T_m=70ºC the relative error reduces to 2%, while for temperatures in the lower range, T_m=30ºC the relative error is 4.2% causing an overestimation of temperature by just 1.3ºC. For the BIPV the relative error of the prediction, as obtained from the results of Fig.11, is: $(T_{PV} - T_m)/T_m = 0.027 - 2.418/T_m$. This, for T_m=50ºC gives a relative error -2.1% and for higher temperature T_m=70ºC the relative error reduces to just -0.8%. Lower PV temperature T_m=30ºC gives a relative error -5.4% which translates to an underestimation of PV temperature by up to 1.6ºC. The model can predict T_{pv} with a small relative error throughout the entire temperature range. The relative error of the prediction by the other models is shown for comparison in Table 3, where it is evident that other models exhibit much larger relative error especially in the high end of the temperature range reaching up to -9.5% causing an underestimation of PV temperature by 6.6ºC in the free-standing PV system and up to 19.2% causing overestimation by 13.4ºC or -18.9% underestimation by 13.2ºC in the BIPV system.

Table 3: Relative error in the prediction of T_{pv} for low, mid, high PV temperatures in comparison to other models

Relative error %	Free-standing PV system			BIPV system		
model	T_{pv}=30°C	T_{pv}=50°C	T_{pv}=70°C	T_{pv}=30°C	T_{pv}=50°C	T_{pv}=70°C
proposed model	4.2	2.6	2.0	-5.4	-2.1	-0.8
King [11]	-5.0	-8.2	-9.5	0.7	13.7	19.2
Mani [36]	5.4	-2.1	-5.3	-10.2	-16.3	-18.9
Faiman [31]	0.5	-6.1	-9.0	-14.4	-16.7	-17.7

An analysis of the predicted ($P_{m,pred}$) vs measured (P_m) power output shows that the relative error of the prediction for the free-standing system, based on the results presented in Fig.8, is: $\left(P_{m,pred} - P_m\right)/P_m = 0.005 + 5.599/P_m$. This, for PV operating with high power output P_m=400W near its nominal value, as it would be during a clear sky day around solar noon, gives a relative error 1.9%, while at low power output P_m=150W during morning/evening hours gives a relative error 4.2%. The slightly higher relative error at low power output may be partly attributed to the slightly higher relative error of T_{pv} prediction at low PV temperatures, while other factors that may contribute are other environmental parameters such as the solar spectrum, angle of incidence of solar irradiance which may have a stronger effect on T_{pv} and P_m prediction during morning and evening hours. The relative error of the Pm prediction is small across the entire power output range.

7. Conclusions

A novel and universally applicable physics based semi-empirical model was developed and validated to predict the PV temperature, T_{pv}, and power output P_m. It is based on a general purpose implicit expression formulated to predict the coefficient *f* which relates T_{pv} with I_T, v_w, T_a, U_{pv}, and the inclination β. The model is a product of 5 functions and may be applied to any flat PV module of any type, age, at any environmental conditions. Regression analysis of the 1st year's monitored data, T_{pv}, T_a, I_T and v_w from a PV sun-tracker with pc-Si modules gave the function $f(v_w)$ which is the main factor affecting *f*, T_{pv} and P_m. The second function accounts for the change $\delta\eta_{pv}$ in the efficiency, and the third for the change δU_{pv} in the heat losses due to the effect of the environmental conditions, (T_a, I_T, v_w), and of the inclination β. The fourth function caters for the PV module natural ageing effect, and the fifth function for the PV module technology to account for the difference in the module efficiency between the module under study and the reference module used for the model development. This is a unique model expressed in compact form, which has integrated:

1.The effect of the environmental factors on the module parameters, T_{pv} and P_m, using an effective approach of perturbation from their SOC values

2.The BIPV,BAPV, BIPV/T mounting design characteristics, using a scaling factor, SF, and

3.The PV module efficiency and operational status as well as the aging effect both compared to the reference PV module used in the model development.

The predicted by this model T_{pv} values were compared for validation purposes with the 2nd year experimental T_{pv} values from a sun-tracking PV system and also with the predictions by 3 well-known models. The relative error in the T_{pv} prediction is small across the entire temperature range. Specifically, for the sun-tracking system the relative error is 2.6% for PV operating temperatures around the NOCT, with a slight increase at lower PV temperatures leading to an overestimation by only 1.3^{o}C. The other models exhibit much larger relative error especially in the high end of the temperature range with an underestimation of PV temperature of up to 6.6^{o}C

This model is also applicable to BIPV configurations introducing a scaling factor SF, which was estimated for this case. A very good agreement was confirmed between predicted by this model and measured T_{pv} in the BIPV case with a very small relative error across the entire temperature range. The relative error is -2.1% for PV temperatures around the NOCT, which increases slightly at lower PV temperatures leading to an underestimation of PV temperature by up to 1.6 ^{o}C. Other models exhibit much larger relative error especially in the high end of the temperature range with an overestimation of PV temperature by 13.4^{o}C or underestimation by 13.2^{o}C. Additionally, this model was used to predict T_{pv} for various BIPV and BAPV configurations operating in USA, Spain and Italy. The predicted T_{pv} was very close to the experimental values, with a performance much higher than other widely used formulas showing the universality of the model.

Finally, the PV power output for the sun-tracking PV array was also predicted based on the T_{pv} model and compared to experimentally determined P_m values giving a relative error 1.9% for PV operating with power output near its nominal value as it would be during a clear sky day around solar noon and a relative error 4.2% at low power output of around 1/3 of its nominal value. All these confirm the wide applicability of this model and its high accuracy in the prediction of *f*, T_{pv} and P_m which was shown to be superior than other widely used models.

References

[1] Skoplaki E. and Palyvos J.A. (2009). On the temperature dependence of photovoltaic module electrical performance: a review of efficiency/power correlations. Solar Energy, vol. 83(5), pp.614–624.

[2] Fuentes M.K. A Simplified Thermal Model for Flat-Plate Photovoltaic Modules, SAND85-0330 UC-63, May 1987

[3] Tina G.M. Marletta G., Sardella S. (2012). Multy-layer thermal models of PV modules for monitoring applications" Proceedings 38th IEEE Photovoltaic Specialists Conference, Austin, Texas, DOI:10.1109/PVSC.2012.6318203.

[4] Kaplanis S. (2016). Determination of the electrical characteristics and thermal behaviour of a c-Si cell under transient conditions for various concentration ratios. Int. J. Sustainable Energy, 35, pp.887-992.

[5] Jones A.D., Underwood P.C. (2001). A Thermal Model for Photovoltaic Systems. Solar Energy, Vol.70(2001)349-359

[6] Armstrong S., Hurley W.G. (2010). A thermal model for photovoltaic panels under varying atmospheric conditions. Applied Thermal Engineering, 30, pp. 1488-1495.

[7] Kaplanis S., Kaplani E. (2019). A New Dynamic Model to Predict Transient and Steady State PV Temperatures Taking into Account the Environmental Conditions. Energies 12 (2019)2

[8] Abdulrazzaq A.K., Plesz B., Bognar G. (2020). A Novel Method for Thermal Modelling of Photovoltaic Modules/Cells under Varying Environmental Conditions. Energies 2020, 13, 3318.

[9] Li C., Spataru S., Zhang K.m Yang Y., Wei H. (2020). A Multi-State Dynamic Thermal Model for Accurate Photovoltaic Cell Temperature Estimation. IEEE Journal of Photovoltaics, DOI:10.1109/JPHOTOV.2020.2987401

[10] Hayes W.,Ngan L. (2014) .A time-dependent model for CdTe PV module temperature in utility-scale systems. IEEE Journal of Photovoltaics, vol. 5(1), pp. 238-242.

[11] King D.L., Boyson W.E., Kratochvill J.A. (2004). Photovoltaic Array Performance Model. SAND2004-3535, December 2004.

[12] Krauter S., Preiss A. (2009). Comparison of Module Temperature Measurement Methods" 34th IEEE Photovoltaic Specialists Conference (PVSC), DOI: 10.1109/PVSC.2009.5411669, Philadelphia, PA, USA.

[13] Skoplaki E., Boudouvis A.G., Palyvos J.A. (2008). A simple correlation of the operating temperature of photovoltaic modules of arbitrary mounting. Solar Energy Materials & Solar Cells, 92, pp.1393-1402

[14] Mattei M. et al. (2006). Calculation of the polycrystalline PV module temperature using a simple method of energy balance. Renewable Energy, vol. 31, no. 4, pp. 553–567.

[15] Trinuruk P., Sorapipatana C.,Chenvidhya D. (2009). Estimating operating cell temperature in BIPV modules in Thailand. Renewable Energy, 34, pp.2515-2523

[16] Siddiqui M.U., Arif A.F., Kelley L., and Dubowsky S. (2012). Three-dimensional thermal modeling of a photovoltaic module under varying conditions, *Solar energy*, vol. 86, no. 9, pp. 2620-2631.

[17] Kaplani E., Kaplanis S. (2014). Thermal modelling and experimental assessment of the dependence of PV module temperature on wind velocity and direction, module orientation and inclination. Solar Energy 107, 443-460.

[18] Hammami M. et al (2017). Thermal and Performance analysis of a Photovolatic Module with an Integrated Energy Storage System. Applied Sciences, Vol 7, 1107; doi: 103390/app7111107

[19] Shahzada P.A. et al. (2018). Using energy balance method to study the thermal behavior of PV panels under time varying field conditions. Energy Conversion and Management, 175, pp.246-262

[20] Migliorini L.,Molinaroli L., Simonetti R., and Manzolini G. (2017). Development and experimental validation of a comprehensive thermoelectric dynamic model of photovoltaic modules. Solar Energy, vol. 144, pp. 489-501.

[21] Kaplani E., Kaplanis S. (2020). Dynamic electro-thermal PV temperature and power output prediction model for any PV geometries in free-standing and BIPV systems operating under any environmental conditions. Energies 2020, 13(18), 4743. https://doi.org/10.3390/en13184743

[22] Graditi G., Ferlito S., Adinolfi G., Tina GM., Ventura C. (2016). Energy yield estimation of thin-film photovoltaic plants by using physical approach and artificial neural networks. Solar Energy Vol. 130, pp.232-243.

[23] Jakhrany A.Q. et al. (2011). Comparison of Solar Photovoltaic Temperature Models. World Applied Sciences Journal 14, (Special Issue of Food and Environment)01-08, 2011, ISSN 1818-4952

[24] Kamuyu W.C.L et al. (2018). Prediction model of Photovoltaic Module Temperature for Power Performance of Floating PVs. Energies 11, 447: doi:103390/en11020447

[25] Duffie J.A., and Beckman W.A. Solar Engineering of Thermal Processes, 3rd Edition, John Wiley and Sons, 2006

[26] Akhasassi M. et al. (2018). Experimental investigation and modeling of the thermal behaviour of a solar PV module. Solar Energy Materials and Solar Cells, 180, pp.271-279

[27] Ross R.G. (1976). Interface design considerations for terrestrial solar cell modules. Proceedings of the 12th IEEE Photovoltaic Specialist’s Conference, Baton Rouge L.A. pp801-806,

[28] Ross R.G. and Smokler M.I. (1986). Electricity from Photovoltaic Solar Cells: Flat-Plate Solar Array project, final Report, Vol.VI, Engineering Sciences and Reliability, Report DOE/JPL-1012-125

[29] Mondol J.D. Yohanis Y.G., Norton B. (2007). Comparison of measured and predicted long term performance of a grid connected Photovoltaic system. Energy Conversion and Management, 48,pp.1065-1080

[30] Servant J.M. (1986). Calculation of the Cell Temperature for Photovoltaic Modules from Climatic Data. Proceedings of the 9th Biennial Congress of ISES- Intersol-85, Montreal, Canada, pp: 370

[31] Faiman D. (2008). Assessing the outdoor operating temperature of photovoltaic modules. Progress in Photovoltaics: Research and Applications, Vol. 16, no. 4, pp. 307–315.

[32] Koehl M. et al. (2011). Modeling of the nominal operating cell temperature based on outdoor weathering. Solar Energy Materials & Solar Cells, 95,pp.1638-1646

[33] Kurtz S. et al. (2009). Evaluation of High-Temperature Exposure of Photovoltaic Modules. NREL/CP-520-45986,June 2009.

[34] Kouadri Boudjelthia E.A. et al. (2016). Role of the wind speed in the evolution of the temperature of the PV module: Comparison of prediction models" Revue des Energies Renouvelables, Vol.19,pp.119-126.

[35] Kalogirou S. Solar Energy Engineering: Processes and Systems. Academic Press, 2009

[36] Mani T.G. et al.(2003). Photovoltaic module thermal/wind performance: Long term monitoring and model development for energy rating. NREL/CD-520-33586, pp936-939

[37] Ciulla G., Lo Brano V., and Moreci E. (2013). Forecasting the cell temperature of PV modules with an adaptive system". International Journal of Photoenergy, Vol. 2013, Article ID 192854.

[38] Schwingshackl C. et al. (2013). Wind effect on PV module temperature: Analysis of different techniques for an accurate estimation. Energy Procedia 40, pp. 77-86.

[39] Kaldellis J., Kapsali M., Kavadias K. (2014). Temperature and wind speed impact on the efficiency of PV installations. Experience obtained from outdoor measurements in Greece. Renewable Energy, 66, pp. 612-624.

[40] Lobera DT., Valkealahti S. (2013). Dynamic thermal model of solar PV systems under varying climatic conditions. Solar Energy, vol. 93, pp. 183-194.

[41] Luketa-hanlin A., Stein JS. (2012). Improvement and validation of a transient model to predict photovoltaic module temperature," Sandia Nat. Lab., Albuquerque, NM, USA, Rep. SAND2012-5509.

[42] Huld T., Gracia Amillo A. M. (2015). Estimating PV module Performance over large Geographical regions: The Role of Irradiance, Air Temperature, Wind Speed and Solar Spectrum. Energies 8, 5159-5181

[43] Biyik E. et al. (2017). A key review of building integrated photovoltaic (BIPV) systems".Engineering science and technology, an international journal, Vol. 20,pp.833-858.

[44] Rosa F. (2020). Building-Integrated Photovoltaics (BIPV) in Historical Buildings: Opportunities and Constraints. Energies, 13(14), 3628.

[45] Agathokleous R.A., Kalogirou S.A.(2016). Double skin facades (DSF) and building integrated photovoltaics (BIPV). A review of configurations and heat transfer characteristics. Renewable Energy 89, pp.743-756

[46] D'Orazio M., Di Perna C., Di Giuseppe E. (2014). Experimental operating cell temperature assessment of BIPV with different installation configurations on roofs under the Mediterranean climate. Renewable Energy, 68, pp. 378-386.

[47] Zhang X. Lau S.K., Lau S.S.Y., et al.. (2018). Photovoltaic integrated shading devices (PVSDs): A review. Solar Energy, 170, 947-968.

[48] Huang C.Y., Chen H.J., Chan C.C. et al. (2011). Thermal model based power-generated prediction by using meteorological data in BIPV system. Energy Procedia, Vol.12, 531-537.

[49] Yang T., Athienitis A.K. (2015). Performance Evaluation of Air-Based Building Integrated Photovolta-ic/Thermal (BIPV/T) System with Multiple Inlets in a Cold Climate. Procedia Engineering, 121, 2060-2067.

[50] Vats K., Tiwari G.N. (2012). Performance evaluation of a building integrated semitransparent photovoltaic thermal system for roof and façade. Energy and Buildings 45, 211-218.

[51] Ghosh A., Sarmah N., Sundaram S., Mallick, T.K. (2019). Numerical studies of thermal comfort for semi-transparent building integrated photovoltaic (BIPV)-vacuum glazing system. Solar Energy 190, 608-616.

[52] Assoa Y.B., Mongibello L., Carr A. et al. (2017). Thermal analysis of a BIPV system by various modelling approaches. Solar Energy 155, 1289-1299.

[53] Huang Y.C., Chan C.-C., Kuan S.-C. et al. (2014). Analysis and monitoring results of a building integrated photovoltaic façade using PV ceramic tiles in Taiwan. International Journal of Photoenergy, Vol.2014, Article ID 615860.

[54] Toledo C., Lopez-Vicente R., Abad J. et al. (2020). Thermal performance of PV modules as building elements: Analysis under real operating conditions of different technologies. Energy and Buildings, 223, 110087.

[55] International Standard IEC 61215. Crystalline silicon terrestrial photovoltaic (PV) modules – design qualification and type approval; 2005.

[56] Justus C.G., Mikhail A. (1976). Height variation of wind speed and wind distribution statistics. Geophysics Res.Lett. 3(5), pp261-264

[57] Saadon S. et al. (2016). Simulation study of a naturally-ventilated building integrated photovoltaic/thermal, BIPV/T, envelope. Renewable Energy 87,pp.517-531

[58] Poulek V. et al. (2018). Influence of increased temperature on energy production of roof integrated PV panels. Energy and Buildings Vol.166, pp 418-425

[59] Muller M.T., Rodriguez J., Marion B. (2009). Performance comparison of a BIPV roofing tile system in two mounting configurations. 34th IEEE Photovoltaic Specialists Conference (PVSC), Philadelphia, USA, pp.000817-22. doi: 10.1109/PVSC.2009.5411159.

[60] Assoa Ya B. et al.(2012). Numerical Analysis of the Impact of Environmental Conditions on BIPV. An Overview of the BIPV Modelling in SOPHIA Project. 27th European Photovoltaic Solar Energy Conference and Exhibition, 2012, Frankfurt, Germany, pp.4143-4149

[61] Gunawan A et al. (2014). The Effect of Building Integration on the Temperature and Performance of Photovoltaic Modules. IEEE 40th Photovoltaic Specialist Conference, 2014, Denver, USA, DOI:10.1109/PVSC.2014.6925033

[62] Yang T., Athienitis A. (2016). A Review of Research and Developments of Building-Integrated Photovoltaic Thermal (BIPV/T) systems" Renewable and Sustainable Energy Reviews 66, issue C, 886-912

[63] DeBlois J.,Bilec M.,Schaefer L. (2013). Simulating home cooling load reduction for a novel opaque roof solar chimney configuration. Applied Energy 112,pp.142-151.

[64] Pantic S., Candanedo L., Athienitis A.K. (2010) Modeling of energy performance of a house with three configurations of building-integrated photovoltaic/thermal systems. Energy and Buildings 42, pp.1779-1789.

[65] Mittelman G., Alshare A.,Davidson J.H.(2009). A model and heat transfer correlation for rooftop integrated photovoltaics with a passive air cooling channel. Solar Energy 83,pp.1150-1160.

[66] Peng C., Yang J. (2016). The effect of Photovoltaic Panels on the Rooftop Temperature in the EnergyPlus Simulation Environment. Intern. J. of Photoenergy, Vol.2016, Article ID:9020567

[67] Kaplanis S., Kaplani E. (eds). Renewable Energy Systems: Theory, Innovations and Intelligent Applications, NOVA Science Publishers, N.Y. 2013.

[68] Brinkworth B.J., Marshall R.H., Ibarahim Z. (2000).A validated model of naturally ventilated PV cladding. Solar Energy 69,pp.67-81

[69] Misara S. Thermal Impacts on Building Integrated Photovoltaics,(BIPV), PhD Thesis 2014 Universitat Kassel, Germany.

[70]Lienhard J.H. IV and Lienhard J.H. V. A Heat Transfer Textbook, Cambridge, Massachusetts, 3rd edition, 2000.

[71] Kayhan O. (2018). A thermal model to investigate the power of solar array for stratospheric balloons in real conditions. Applied Thermal Engineering 139,pp.113-120

[72] Bardhi M., Grandi G. and Tina G.M. (2012). Comparison of PV cell temperature Estimation by Different Thermal Power Exchange Calculation Methods" Proc. ICREPQ`12, Santiago de Compostella, (Spain), 28-30 March, 2012.

[73] Siegel R., Howell J.R. Thermal Radiation Heat Transfer. Taylor & Francis, 2002

[74] Kreith F. Principles of Heat Transfer. International Textbook Company, Penn.,(1961)330-331

[75] Shurcliff W.A. (1974). Transmittance and reflection loss of multi-plate planar window of a solar radiation collector. J Solar Energy, Vol. 16, pp149-154

[76]Bazilian M. D., Kamalanathan H., Prasad D.K. (2002). Thermographic analysis of a building integrated photovoltaic system. Renewable Energy 26(3), pp.449-461

[77] Karava P., Jubayer CM., Savory E, Li S. (2012). Effect of incident flow conditions on convective heat transfer from the inclined windward roof of a low-rise building with application to photovoltaic-thermal systems. J Wind Eng Ind Aerod Vol. 104–106, pp428-438

[78] Evans D.L. (1981). Simplified Method for Predicting Photovoltaic Array Output. Solar Energy 27,pp.555-460.

[79] Anderson, A.J. (1996). Photovoltaic Translation Equations: A New Approach. Final Subcontract Report NREL/TP-411-20279; Office of Scientific and Technical Information (OSTI): Oak Ridge, TN, USA.

APPENDIX

1. $\eta_{pv,SOC}$ is the efficiency η_{pv} at SOC with T_a =20°C, I_T=800W/m^2, considering v_w<1 m/s. According to [78]:

$$\eta_{pv,SOC} = \eta_{pv,STC}\left(1 + \gamma\left(T_{pv,SOC} - 25^{o}C\right) + \delta \cdot ln\left(\frac{800}{10^3}\right)\right) \tag{A.1}$$

Parameters $\gamma=\vartheta\eta_{pv}/\vartheta T_{pv}$ and δ depend on the PV cell technology. The values for c-Si are -0.005K^{-1} and 0.11, respectively. $\eta_{pv,STC}$ is the efficiency at STC in the present status of the module.

2. $T_{pv,SOC}$ in (A.1) is estimated by:

$$T_{pv,SOC} = 20^{o}C + f(v_w = 0)800W/m^2, \text{ the higher order terms in eq.(20) are dropped} \tag{A.2}$$

3. $$\delta T_{pv} = T_{pv} - T_{pv,SOC} = T_a + f(v_w)I_T - T_{pv,SOC} \tag{A.3}$$

4. The infinitesimal change $\delta\eta_{pv}$ may be estimated by:

$$\delta\eta_{pv} = \left(\frac{\vartheta\eta_{pv}}{\vartheta T_{pv}}\right)\delta T_{pv} + \left(\frac{\vartheta\eta_{pv}}{\vartheta I_T}\right)\delta I_T \tag{A.4}$$

the first term was given above and the second one is estimated as below.

5. $(\vartheta\eta_{pv}/\vartheta I_T)\ \delta I_T$ is determined by the following expression using eq.(A.1) and eq.(14)

$$\left(\frac{\partial\eta_{pv}}{\partial I_T}\right)\delta I_T = \eta_{pv,SOC}\left(\frac{1}{I_T}\delta + \gamma f + \gamma\frac{dT_a}{dI}\right)\left(I_T - I_{T,SOC}\right) \tag{A.5}$$

dT_a/dI depends on the local climate and season and may be taken equal to 1-2°C/100W/m^2. Eq.(A.5) implies positive and negative contribution during the day and depends on the I_T, f and dT_a/dI_T. The contribution of $\partial\eta_{pv}/\partial I_T$ to the f prediction is negligible for I_T around $I_{T,SOC}$= 800W/m^2.

4. The following expressions provide the average values of the rates of change for U_{pv} with respect to T_{pv} and β for natural air flow when the dependence of *f* on T_{pv} and β is essential, eq.(20). At forced flow conditions the terms below take negligible values and the *f* is predicted by eq.(22).

$$\left(\frac{\partial U_f}{\partial T}\right)\delta T_{pv} = \frac{\partial\left(h_{c,f}+h_{r,f}\right)}{\partial T}\delta T_{pv} = 0.065\cdot\delta T_{pv} \quad \text{(A.6a)}$$

$$\left(\frac{\partial U_b}{\partial T}\right)\delta T_{pv} = \frac{\partial\left(h_{c,b}+h_{r,b}\right)}{\partial T}\delta T_{pv} = 0.062\cdot\delta T_{pv} \quad \text{(A.6b)}$$

$$\left(\frac{\partial U_f}{\partial \beta}\right)\delta\beta = \frac{\partial\left(h_{c,f}+h_{r,f}\right)}{\partial \beta}\delta\beta = -0.0074\cdot\delta\beta \quad \text{(A.6c)}$$

$$\boldsymbol{\left(\frac{\partial U_b}{\partial \beta}\right)\delta\beta = \frac{\partial\left(h_{c,b}+h_{r,b}\right)}{d\beta}\delta\beta = 0.0195\cdot\delta\beta}$$

(A.6d)

where $\delta\beta = \beta - \varphi$

Declaration of interests

☒ The authors declare that they have no known competing financial interests or personal relationships that could have appeared to influence the work reported in this paper.

☐The authors declare the following financial interests/personal relationships which may be considered as potential competing interests: